PLOS ONE

RESEARCH ARTICLE

iPLA$_2$-VIA is required for healthy aging of neurons, muscle, and the female germline in *Drosophila melanogaster*

Surya Jyoti Banerjee‡, Adina Schonbrun‡, Sogol Eizadshenass, Shimshon Benji, Yaakov Tzvi Cantor, Liam Eliach, Matthew Lubin, Zev Narrowe, Jeremy Purow, Benjamin Shulman, Leib Wiener, Josefa Steinhauer*

Department of Biology, Yeshiva University, New York, NY, United States of America

‡ These authors are co-first authors on this work.
* jsteinha@yu.edu

Citation: Banerjee SJ, Schonbrun A, Eizadshenass S, Benji S, Cantor YT, Eliach L, et al. (2021) iPLA$_2$-VIA is required for healthy aging of neurons, muscle, and the female germline in *Drosophila melanogaster*. PLoS ONE 16(9): e0256738. https://doi.org/10.1371/journal.pone.0256738

Editor: Subhabrata Sanyal, Calico LLC, UNITED STATES

Received: August 4, 2021

Accepted: August 13, 2021

Published: September 10, 2021

Data Availability Statement: All relevant data are within the manuscript and its Supporting Information files.

Funding: HHS | NIH | Eunice Kennedy Shriver National Institute of Child Health and Human Development (NICHD): Josefa M. Steinhauer R15-HD080511.

Competing interests: The authors declare that they have no conflict of interest.

Abstract

Neurodegenerative disease (ND) is a growing health burden worldwide, but its causes and treatments remain elusive. Although most cases of ND are sporadic, rare familial cases have been attributed to single genes, which can be investigated in animal models. We have generated a new mutation in the calcium-independent phospholipase A_2 (iPLA$_2$) VIA gene *CG6718*, the *Drosophila melanogaster* ortholog of human *PLA2G6/PARK14*, mutations in which cause a suite of NDs collectively called *PLA2G6*-associated neurodegeneration (PLAN). Our mutants display age-related loss of climbing ability, a symptom of neurodegeneration in flies. Although phospholipase activity commonly is presumed to underlie iPLA$_2$-VIA function, locomotor decline in our mutants is rescued by a transgene carrying a serine-to-alanine mutation in the catalytic residue, suggesting that important functional aspects are independent of phospholipase activity. Additionally, we find that iPLA$_2$-VIA knockdown in either muscle or neurons phenocopies locomotor decline with age, demonstrating its necessity in both neuronal and non-neuronal tissues. Furthermore, RNA in situ hybridization shows high endogenous *iPLA$_2$-VIA* mRNA expression in adult germ cells, and transgenic HA-tagged iPLA$_2$-VIA colocalizes with mitochondria there. Mutant males are fertile with normal spermatogenesis, while fertility is reduced in mutant females. Mutant female germ cells display age-related mitochondrial aggregation, loss of mitochondrial potential, and elevated cell death. These results suggest that iPLA$_2$-VIA is critical for mitochondrial integrity in the *Drosophila* female germline, which may provide a novel context to investigate its functions with parallels to PLAN.

Introduction

As global population demographics have shifted toward older age, neurodegenerative disease (ND) has become an increasing health burden worldwide [1]. Treatment has been confounded by the fact that loss of neurons in ND, which leads to dementia and reduced motor control, is

Abbreviations: PLA$_2$, Phospholipase A$_2$; iPLA$_2$-VIA, calcium-independent phospholipase A$_2$-VIA; CL, cardiolipin; PC, phosphatidylcholine; PE, phosphatidylethanolamine; ER, endoplasmic reticulum; IC, spermatid individualization complex; PLAN, *PLA2G6*-associated neurodegeneration.

associated with numerous cytopathologies, including DNA damage and epigenetic changes, mitochondrial and lysosomal dysfunction, Ca^{+2} dysregulation, disrupted RNA and protein homeostasis, as well as inflammation [1, 2]. Thus, there is a pressing need to better understand the underlying drivers of ND.

Parkinson's disease is the second most common ND, affecting ~1% of individuals over the age of 60 [3]. Most cases of Parkinson's disease are sporadic, presumably arising from a complex interplay between genotype and environment. In some cases, though, environmental toxins have been identified as direct causative agents. For example, contamination of the synthetic opioid MPPP (1-methyl-4-phenyl-4-propionoxy-piperidine) with MPTP (1-methyl-4-phenyl-1,2,3,6-tetrahydropyridine), which is metabolized to MPP^+ (1-methyl 4-pyridinium) in vivo, caused a cluster of acute cases of parkinsonism amongst opiate users [4]. The herbicide paraquat and the pesticide rotenone also have been linked to the disease [5, 6]. These toxins inhibit the electron transport chain and promote oxidative stress, suggesting that mitochondrial dysfunction is central, and potentially causative in some cases, to the disease pathology [7, 8].

Several inherited disorders that bear striking resemblance to Parkinson's disease have permitted identification of genetic contributors, the so-called *PARK* genes [9]. Many of these genes encode products that can localize to mitochondria and affect mitochondrial activity and quality control, again suggesting a key role for mitochondrial integrity in the disease and positioning it as a potential therapeutic target [7, 10]. *PLA2G6/PARK14* encodes the group 6A calcium-independent phospholipase A$_2$ (iPLA$_2$-VIA, also called iPLA$_2$-β). In 2006, this gene was linked to a group of severe NDs, including infantile neuroaxonal dystrophy and neurodegeneration with brain iron accumulation, and three years later was found to be associated with an autosomal recessive dystonia-parkinsonism [11–14].

The iPLA$_2$-VIA enzyme, like other PLA$_2$s, hydrolyzes fatty acyl chains from the *sn-2* position of glycerophospholipids [15]. Acting within the Lands Cycle of deacylation and reacylation, PLA$_2$s promote phospholipid remodeling and repair [16]. Acyl chain remodeling seems to be especially important for the mitochondrial phospholipid cardiolipin (CL), which is highly susceptible to oxidative damage due to its proximity to the electron transport chain. In the absence of remodeling, accumulation of damaged CL acyl chains is thought to reduce respiratory function and promote oxidative stress and apoptosis [17, 18]. iPLA$_2$-VIA can localize to mitochondria in several mammalian cell types and has been implicated in CL remodeling [19–25]. Moreover, *PLA2G6* mutant animal models display features of ND along with mitochondrial abnormalities, suggesting the possibility that *PLA2G6*-associated neurodegeneration (PLAN) arises from mitochondrial dysfunction in the absence of CL repair [26–29]. However, dramatic CL molecular changes have not been found consistently in *PLA2G6* mutant models [26, 27, 30], raising questions of how important iPLA$_2$-VIA is for CL remodeling and whether this molecular process underlies PLAN.

iPLA$_2$-VIA hydrolyzes other phospholipids in addition to CL and can generate lipid signaling mediators [31]. iPLA$_2$-VIA also bears near its N-terminus 8–9 ankyrin repeats, which can serve as protein-protein interaction domains, although critical interactors have yet to be characterized [32]. It has been observed in a variety of subcellular locations and has been implicated in numerous cellular activities, including cell cycle progression, vesicle trafficking, Ca^{+2} homeostasis, ER stress, and apoptosis [15, 21, 31, 33–35]. The relationships between iPLA$_2$-VIA's molecular, cellular, and physiological functions currently are unclear. We investigated *iPLA$_2$-VIA* in *Drosophila melanogaster* by determining its endogenous expression pattern and generating a new null mutant. *iPLA$_2$-VIA* is expressed ubiquitously at low levels in imaginal tissues. Null mutants are viable and show no synthetic lethality or sterility with two key phosphatidylcholine (PC) metabolizing enzymes. Consistent with a number of recent reports, null

iPLA$_2$-VIA mutants show a striking decline in locomotor ability with age [26, 36, 37], which surprisingly can be rescued by a catalytic-dead iPLA$_2$-VIA transgene. Whereas prior reports have focused on neurons, for the purpose of modeling ND, we show here that the locomotor decline can be phenocopied with either neuronal-specific or muscle-specific knockdown, indicating the importance of this gene in multiple adult tissue types. Furthermore, high endogenous expression is observed in both male and female adult germ cells, and transgenic HA-tagged iPLA$_2$-VIA-PB localizes prominently to mitochondria there. Although the mammalian homolog has been implicated in male fertility [38], we observe normal fertility and spermatogenesis in male *iPLA$_2$-VIA* mutant *Drosophila*. Still, female mutants have reduced fertility, with age-dependent abnormal mitochondrial aggregation, reduced mitochondrial potential, and elevated cell death in the germline. Taken together, our results demonstrate that iPLA$_2$-VIA activity in both neurons and muscles protects from age-related locomotor decline but implicate putative non-catalytic mechanisms in its protective function. We also show that iPLA$_2$-VIA is important for mitochondrial integrity in the *Drosophila* female germline.

Results

A null iPLA$_2$-VIA mutation does not interact genetically with phospholipid metabolism genes

The *Drosophila melanogaster iPLA$_2$-VIA (CG6718)* locus encodes four predicted transcripts and two protein isoforms, which differ by 13 amino acids at their N termini (Fig 1A). Both *Drosophila* isoforms are highly similar to mammalian iPLA$_2$-VIA, with a conserved ankyrin repeat region, catalytic residues, and a 1-9-14 calmodulin binding motif (Fig 1B, [32], the *Drosophila* PA isoform shares 48% similarity and the PB isoform 47.5% similarity with the shorter human iPLA$_2$-VIA protein, and they are 50.4% and 49.9% similar to the longer human isoform, respectively). To generate a genomic mutation in *Drosophila iPLA$_2$-VIA*, we excised the P element EY5103 and isolated a 1.4 kb deletion, called *iPLA$_2$-VIA$^{\Delta 23}$*, that spans the transcription initiation site as well as both predicted translation start codons (Fig 1A). Reverse transcription (RT)—PCR confirmed the absence of full-length *iPLA$_2$-VIA* mRNA in our mutant, while the EY5103 insertion line retains a low level of *iPLA$_2$-VIA* transcript (Fig 1C, see also [36]). The null mutants are homozygous and hemizygous viable at room temperature (Table 1) but have reduced lifespans (not shown), as reported in previous studies [26, 36, 39].

Early studies implicated iPLA$_2$-VIA in phospholipid homeostasis [33]. For example, overexpressing the phosphatidylcholine (PC) synthesis enzyme CDP phosphocholine cytidylyltransferase (Pcyt1) in mammalian cells led to compensatory upregulation of iPLA$_2$-VIA expression and activity, to catabolize the excess PC [40, 41]. To explore whether this role is conserved at the organismal level in *Drosophila*, we used the *EP* line *GS15374* to overexpress Pcyt1 with the ubiquitously expressed *tubulin-GAL4* driver. After confirming *Pcyt1* overexpression by RT-PCR (S1A Fig, bottom gel panel), we examined *iPLA$_2$-VIA* mRNA levels. In whole flies, *iPLA$_2$-VIA* mRNA expression does not increase when Pcyt1 is overexpressed (S1A Fig). We confirmed this result using RT-qPCR (S1E Fig). Additionally, no lethality is observed when Pcyt1 is overexpressed in the *iPLA$_2$-VIA$^{\Delta 23}$* mutant (Table 2A), indicating that iPLA$_2$-VIA is not necessary for survival upon Pcyt1 overexpression. We also tested for genetic interactions between our *iPLA$_2$-VIA$^{\Delta 23}$* mutation and a *pcyt1* loss of function allele that reduces PC levels [42], reasoning that removing *iPLA$_2$-VIA* from the *pcyt1* mutant might partially suppress its phenotype by allowing more PC to accumulate. However, neither the lethality nor the sterility of *pcyt1^{16919}* mutants is suppressed by the absence of *iPLA$_2$-VIA* (Table 2B–2D), and iPLA$_2$-VIA mRNA levels are not reduced in *pcyt1* mutant flies (S1B Fig, RT-qPCR shown in S1F Fig). Sws/NTE is a phospholipase in the same family as iPLA$_2$-VIA and is known to be

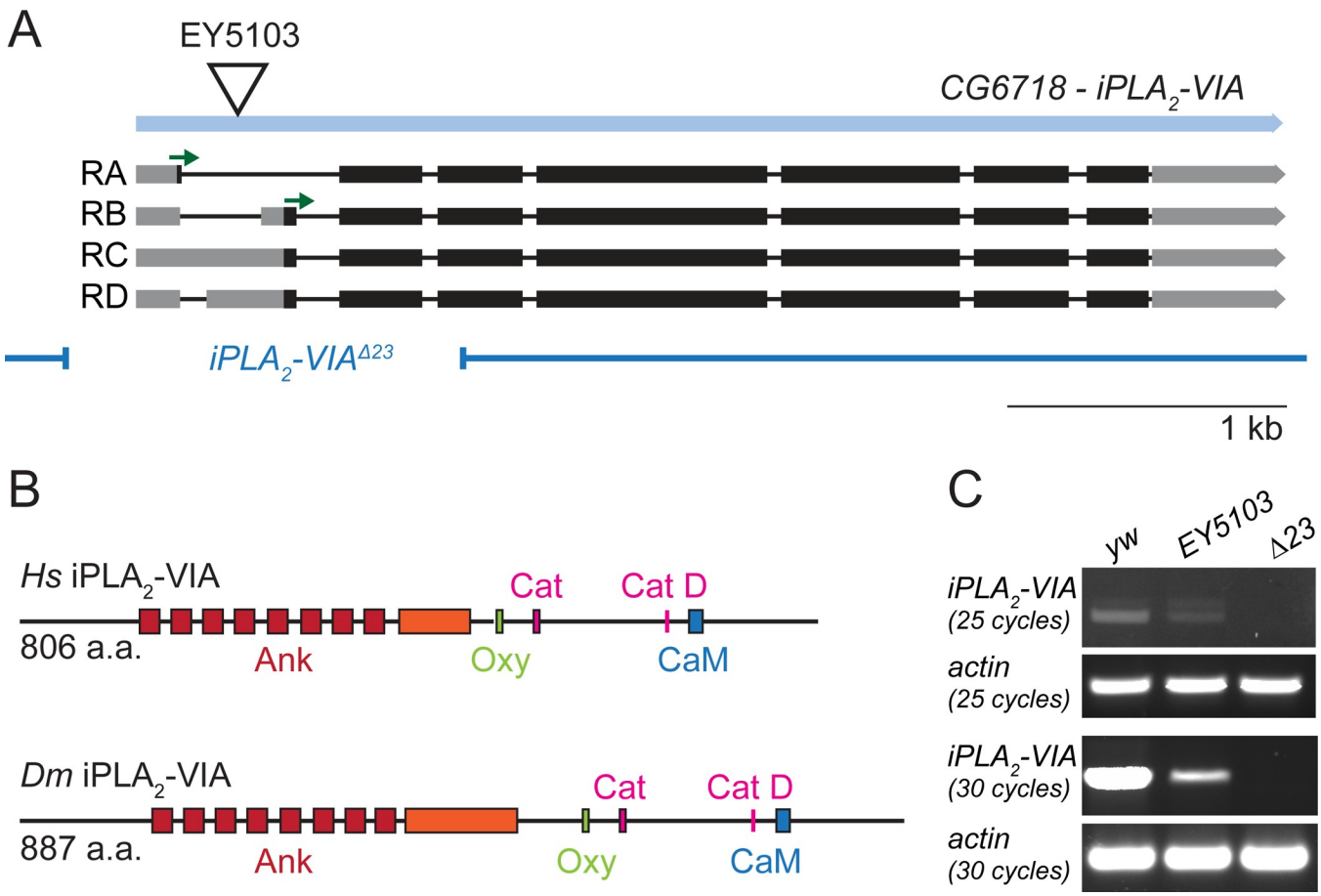

Fig 1. A new mutant allele of *Drosophila iPLA$_2$-VIA*. (A) Map of the *CG6718 iPLA$_2$-VIA* gene (light blue) showing the insertion site of the EY5103 P element (triangle), predicted transcripts with start codons (green arrows), and the 1.4 kb Δ23 deletion (breakpoints indicated by the dark blue lines). (B) Domain mapping of primary structures demonstrates high homology between *Drosophila* and human iPLA$_2$-VIA. Colors are as in [32], with red indicating the ankyrin repeats (Ank; the ninth ankyrin repeat in the shorter mammalian iPLA$_2$-VIA isoform is disrupted by additional residues in the fly proteins and in the longer mammalian iPLA$_2$-VIA isoform, indicated here in orange), green indicating the oxyanion hole that coordinates the substrate during catalysis (Oxy), pink indicating the catalytic site (Cat, GTSTG) and catalytic aspartate residue (Cat D), and blue indicating the 1-9-14 calmodulin binding motif (CaM). (C) Whole fly RT-PCR demonstrates the absence of full-length *iPLA$_2$-VIA* mRNA in the Δ23 mutant. The EY5103 insertion line retains low levels of *iPLA$_2$-VIA* mRNA.

https://doi.org/10.1371/journal.pone.0256738.g001

important for PC homeostasis [43]. Loss of *iPLA$_2$-VIA* does not enhance the lethality of *sws*^{4} mutants (Table 3), suggesting that iPLA$_2$-VIA does not compensate for Sws/NTE in processes that affect viability. Finally, *iPLA$_2$-VIA* mRNA expression is unchanged in whole flies mutant for the ethanolamine kinase *easily shocked (eas)*, a key enzyme in phosphatidylethanolamine (PE) synthesis (S1C Fig, RT-qPCR shown in S1G Fig, [44]). All together, our results do not point to a major unique role for *Drosophila* iPLA$_2$-VIA in phospholipid housekeeping, although our results do not preclude important roles in specific tissues. Publicly available high-throughput expression data confirm that *pcyt1*, *sws*, and *eas* all show moderate to high expression throughout the organism, in embryonic, larval, and adult stages (flybase.org).

iPLA$_2$-VIA in neurons and muscles maintains locomotor ability with age, via a partially catalytic-independent activity

Because *iPLA$_2$-VIA* is associated with ND in humans, we tested our mutant flies for their climbing ability, which is known to decline with age under conditions of neurodegeneration

Table 1. *iPLA$_2$-VIA$^{\Delta 23}$* mutants are viable.

A. *iPLA$_2$-VIA$^{\Delta 23}$* sib-mate			
	Observed	Expected	Viability
Homozygotes	73	64	114%
Balancer siblings	128		
		p =	*0.260*
B. *iPLA$_2$-VIA$^{\Delta 23}$* x *Df(3L)BSC394*			
	Observed	Expected	Viability
Hemizygotes	105	99	106%
Balancer siblings	99		
		p =	*0.546*
C. *iPLA$_2$-VIA$^{\Delta 23}$* x *Df(3L)BSC282*			
	Observed	Expected	Viability
Hemizygotes	126	138	91%
Balancer siblings	138		
		p =	*0.307*

iPLA$_2$-VIA$^{\Delta 23}$ mutants are homozygous (A) and hemizygous (B, C) viable. Numbers are F1 progeny ("observed"). Expected numbers are derived from the observed number of balancer siblings and the expected Mendelian ratios. "Viability" represents the proportion of observed homozygous or hemizygous F1 flies compared to the expected number. Statistical comparison by chi-square test.

https://doi.org/10.1371/journal.pone.0256738.t001

[45]. In accord with other reports, *iPLA$_2$-VIA$^{\Delta 23}$* mutants exhibit climbing defects after 20 days of age, in contrast to background control and isogenic control animals (Fig 2A and 2B, light bars [26, 36, 39]). Ubiquitous expression of a C-terminally HA-tagged iPLA$_2$-VIA-PB wild-type cDNA transgene rescues the climbing ability of the mutant, confirming the locus-specificity of the defect (Fig 2C and 2D, dark bars). We additionally constructed an iPLA$_2$-VIA-PB cDNA transgene in which the catalytic serine is replaced with an alanine residue (called iPLA$_2$-VIA-PB SA), a well characterized alteration that abrogates catalytic activity [32, 46, 47]. Surprisingly, the catalytic-dead transgene also rescues the climbing defect of mutant flies, suggesting that iPLA$_2$-VIA function is at least partially independent of catalytic activity (Fig 2C and 2D, yellow bars, [32]). Although the wild-type and catalytic-dead transgenes are identical apart from the catalytic serine, and they are inserted into the same genomic locus, expression of the catalytic-dead protein appears ~50% weaker than the wild-type protein on a Western blot (S2 Fig). This might indicate reduced stability of the mutant protein. Thus, the lower rescuing activity of the catalytic-dead transgene may be due to reduced protein levels and/or to functions associated with the catalytic residue.

Ubiquitous RNAi knockdown of *iPLA$_2$-VIA* using *tubulin-GAL4* phenocopies the mutant in both males (Fig 2E, gray bars) and females (Fig 2F, gray bars). Knocking down *iPLA$_2$-VIA* only in neurons with the *elav-GAL4* driver produces a climbing defect that is markedly weaker than in the ubiquitous knockdown (Fig 2G and 2H), suggesting a requirement in additional tissues other than neurons. In accord with this, RNAi knockdown of *iPLA$_2$-VIA* with the muscle-specific driver *DJ667-GAL4* also reproduces the climbing defect (Fig 2I and 2J, gray bars). In comparison to knockdown of *pink1*, a gene required for maintenance of muscle integrity with age (Fig 2I and 2J, red bars, [48, 49]), *iPLA$_2$-VIA* knockdown is comparable at 20 days in males and even stronger by 30 days of age in both males and females. Thus, iPLA$_2$-VIA is required in neurons and muscle, and possibly other tissues, for maintenance of normal locomotor activity with age. Publicly available high throughput transcriptomic data show moderate to strong expression also in gut, fat body, and heart, all tissues known to affect aging (flybase.org; [50]).

Table 2. *iPLA$_2$-VIA* and *pcyt1* do not show synthetic effects on viability or fertility.

A. *Pcyt1 overexpression*	Observed	Expected	Viability
tub-GAL4 > UAS-pcyt1; iPLA$_2$-VIA$^{\Delta 23}$	48	45	107%
UAS-pcyt1; iPLA$_2$-VIA$^{\Delta 23}$	45		
		p =	*0.655*
tub-GAL4 > UAS-pcyt1; iPLA$_2$-VIA^{+}	29	29	100%
UAS-pcyt1; iPLA$_2$-VIA^{+}	29		
		p =	*1.00*

B.	***pcyt1^{16919} iPLA$_2$-VIA$^{\Delta 23}$* sib-mate**			***pcyt1^{16919}* sib-mate**		
	Observed	Expected	Viability	Observed	Expected	Viability
Homozygotes	29	63.5	46%	21	41	51%
Balancer siblings	127			82		
					p =	*0.720*

C.	***pcyt1^{16919} iPLA$_2$-VIA$^{\Delta 23}$* females** (n = 10)	***pcyt1^{16919}* females** (n = 9)
Average number of progeny	0	0

D.	***pcyt1^{16919} iPLA$_2$-VIA$^{\Delta 23}$* males** (n = 10)	***pcyt1^{16919}* males** (n = 10)
Average number of progeny	0.4 ± 0.843	1.6 ± 2.55
		p = 0.185

(A) Overexpressing Pcyt1 does not cause lethality in a control background or in the *iPLA$_2$-VIA$^{\Delta 23}$* mutant. Numbers of flies overexpressing Pcyt1 and sibling flies lacking the *tubulin-GAL4* driver are shown. "Viability" represents the proportion of overexpressing flies compared to the matched siblings without the *tubulin-GAL4* driver. Statistical comparison by chi-square test. (B) Although *pcyt1^{16919}* homozygotes are sub-viable, *pcyt1^{16919} iPLA$_2$-VIA$^{\Delta 23}$* double mutants show no additional lethality. Numbers shown are F1 progeny ("observed") from mated heterozygous parents. Expected numbers are derived from the observed number of balancer siblings and the expected Mendelian ratios. "Viability" represents the proportion of observed homozygous F1 flies compared to the expected number. The proportion of *pcyt1^{16919}* homozygotes was compared to the proportion of *pcyt1^{16919} iPLA$_2$-VIA$^{\Delta 23}$* double mutant homozygotes using two proportion z-test. (C) Both *pcyt1^{16919}* homozygous females and *pcyt1^{16919} iPLA$_2$-VIA$^{\Delta 23}$* double mutant homozygous females are completely sterile in individual crosses to single *yw* males at 23˚C. Crosses were kept and monitored for signs of progeny for 8–10 days. (D) Both *pcyt1^{16919}* homozygous males and *pcyt1^{16919} iPLA$_2$-VIA$^{\Delta 23}$* double mutant homozygous males are markedly sub-fertile in individual crosses to single *yw* females at 23˚C. Parental mating pairs were kept for 8–10 days. Average number of progeny from individual crosses shown ± standard deviations, comparison by unpaired t-test.

https://doi.org/10.1371/journal.pone.0256738.t002

Drosophila iPLA$_2$-VIA is expressed strongly in adult germline but is not required for spermatogenesis

To explore further the endogenous expression of *Drosophila iPLA$_2$-VIA*, we performed RNA in situ hybridization. We observe weak mRNA expression in wild-type imaginal tissues and no

Table 3. *iPLA$_2$-VIA* and *sws* do not show synthetic loss of viability.

	***sws^4 iPLA$_2$-VIA$^{\Delta 23}$* sib-mate**		
	Observed	**Expected**	**Viability**
Double mutant	26	34	76%
iPLA$_2$-VIA mutant	34		
sws mutant	70	81	86%
Balancer siblings	81		
		p =	*0.691*

Although *sws^4* mutants are sub-viable, *sws^4 iPLA$_2$-VIA$^{\Delta 23}$* double mutants show no additional lethality. Numbers shown are F1 progeny ("observed") from mated heterozygous parents (male parents are heterozygous for *iPLA$_2$-VIA$^{\Delta 23}$* but hemizygous for *sws^4*). Expected numbers are derived from the observed number of balancer siblings and the expected Mendelian ratios. "Viability" represents the proportion of observed mutant F1 flies compared to the expected number. Proportion of *sws^4 iPLA$_2$-VIA$^{\Delta 23}$* double mutants versus *iPLA$_2$-VIA$^{\Delta 23}$* single mutants was compared to the proportion of sibling *sws^4* mutants versus balancer controls using two proportion z-test.

https://doi.org/10.1371/journal.pone.0256738.t003

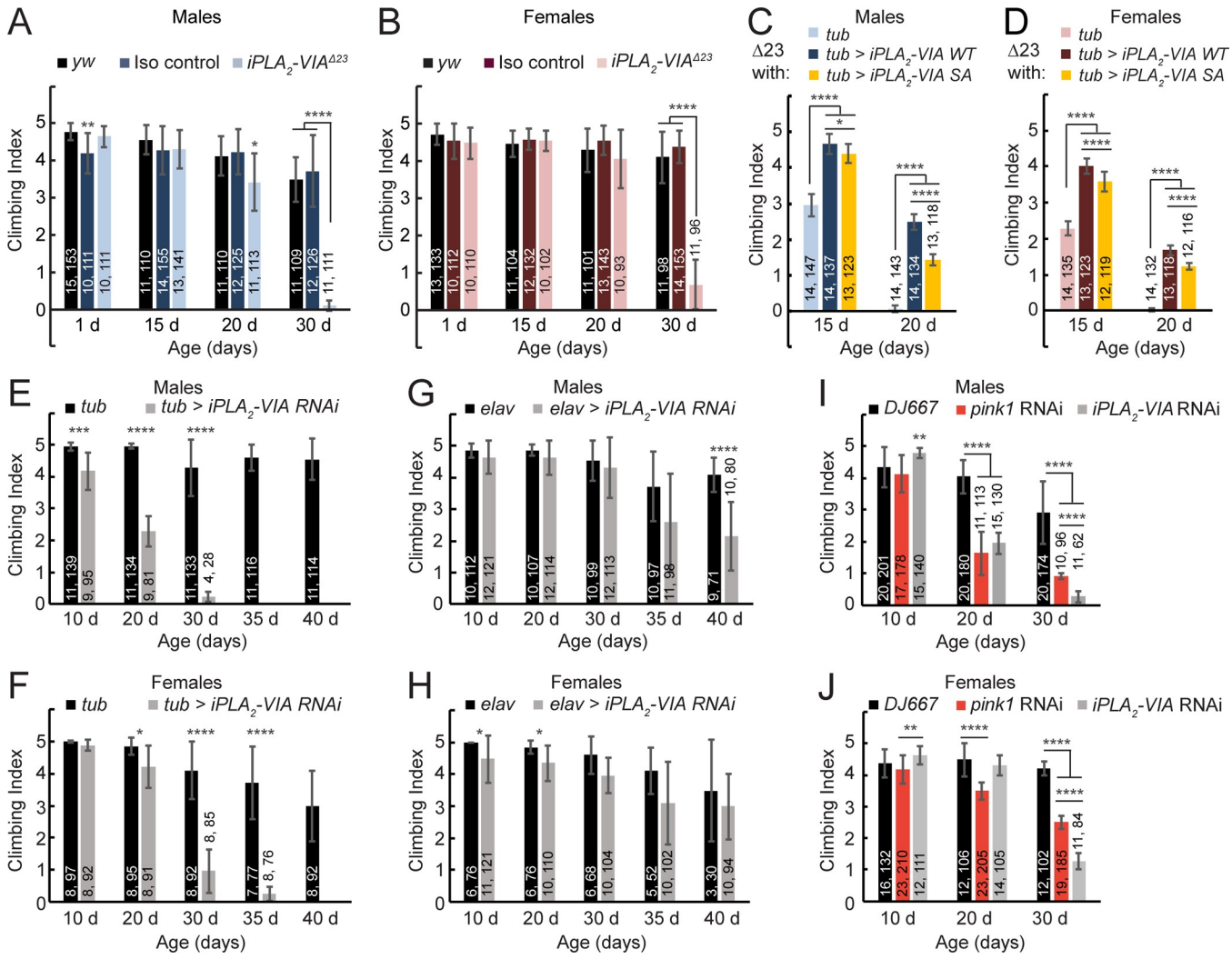

Fig 2. Impaired climbing ability in aged *iPLA$_2$-VIA$^{\Delta 23}$* mutants can be rescued by a catalytic dead *iPLA$_2$-VIA-PB* transgene and phenocopied with neuronal or muscle knockdown. (A-B) Male (A, light blue) and female (B, light pink) *iPLA$_2$-VIA$^{\Delta 23}$* mutant adults have normal climbing ability until 20 days of age at room temperature. After 20 days, climbing ability declines compared to *yw* (black) and isogenic controls (dark blue in A, and dark red in B). Newly eclosed isogenic control males (A, dark blue) show slightly reduced climbing ability compared to *yw* males. (C-D) *Tubulin-GAL4* driven expression of wild-type *UAS-iPLA$_2$-VIA-HA* in males (C, dark blue bars) and females (D, dark red bars) at 26˚C rescues the climbing defect of aged *iPLA$_2$-VIA$^{\Delta 23}$* mutants at 15 and 20 days of age. 26˚C was used to increase GAL4 activity in rescue and knockdown experiments. Note that mutant flies show climbing defects by 15 days at this higher temperature. In this experiment, mutants carry the GAL4 driver without the resue transgene (light blue bars in C, and light pink bars in D). *Tubulin-GAL4* driven expression of a *UAS-iPLA$_2$-VIA-SA* transgene carrying a serine-to-alanine mutation in the catalytic residue at 26˚C also partially rescues the climbing defect (yellow bars), although rescue is weaker than with the wild-type transgene. Wild-type and SA transgenes were transformed into the same genomic locus using the phi-C31 system. (E-F) Ubiquitous expression of *UAS*-driven double stranded RNA targeting *iPLA$_2$-VIA* (*HMS01544*) with *tubulin-GAL4* at 26˚C phenocopies the climbing defect in male (E) and female (F) flies (gray bars, compared to *GAL4*-only controls, black bars). Knockdown flies die by 35 and 40 days of age in males and females, respectively. (G-H) Expressing *HMS01544* in neurons only with *elav-GAL4* at 26˚C weakly phenocopies the climbing defect in male (G) and female (H) flies (gray bars, compared to *GAL4*-only controls, black bars). (I-J) Expressing *HMS01544* in muscles only with *DJ667-GAL4* produces a strong phenocopy of the age-induced climbing defect in male (I) and female (J) flies, similar to that resulting from knockdown of *pink1 (HMS02204*, red bars). Note that *pink1* knockdown flies also have moderately reduced climbing ability at 10 days of age compared to *iPLA$_2$-VIA* knockdown flies, but this was not statistically significant compared to GAL4-only controls. Number of groups (first number) and number of flies (second number) assayed for each condition is shown on the graphs. Bars represent the average climbing index for each condition. Error bars are standard deviations. Differences assessed by unpaired t-test, $^{*}p < 0.05$, $^{**}p < 0.01$, $^{***}p < 0.005$, $^{****}p < 0.0005$.

https://doi.org/10.1371/journal.pone.0256738.g002

detectable expression in wild-type larval brains (Fig 3A–3F). Strikingly, strong expression is seen in the germ cells of both male and female adults (Fig 3G and 3H). Because iPLA$_2$-VIA has been implicated previously in mammalian male fertility [38], we examined male fertility in our

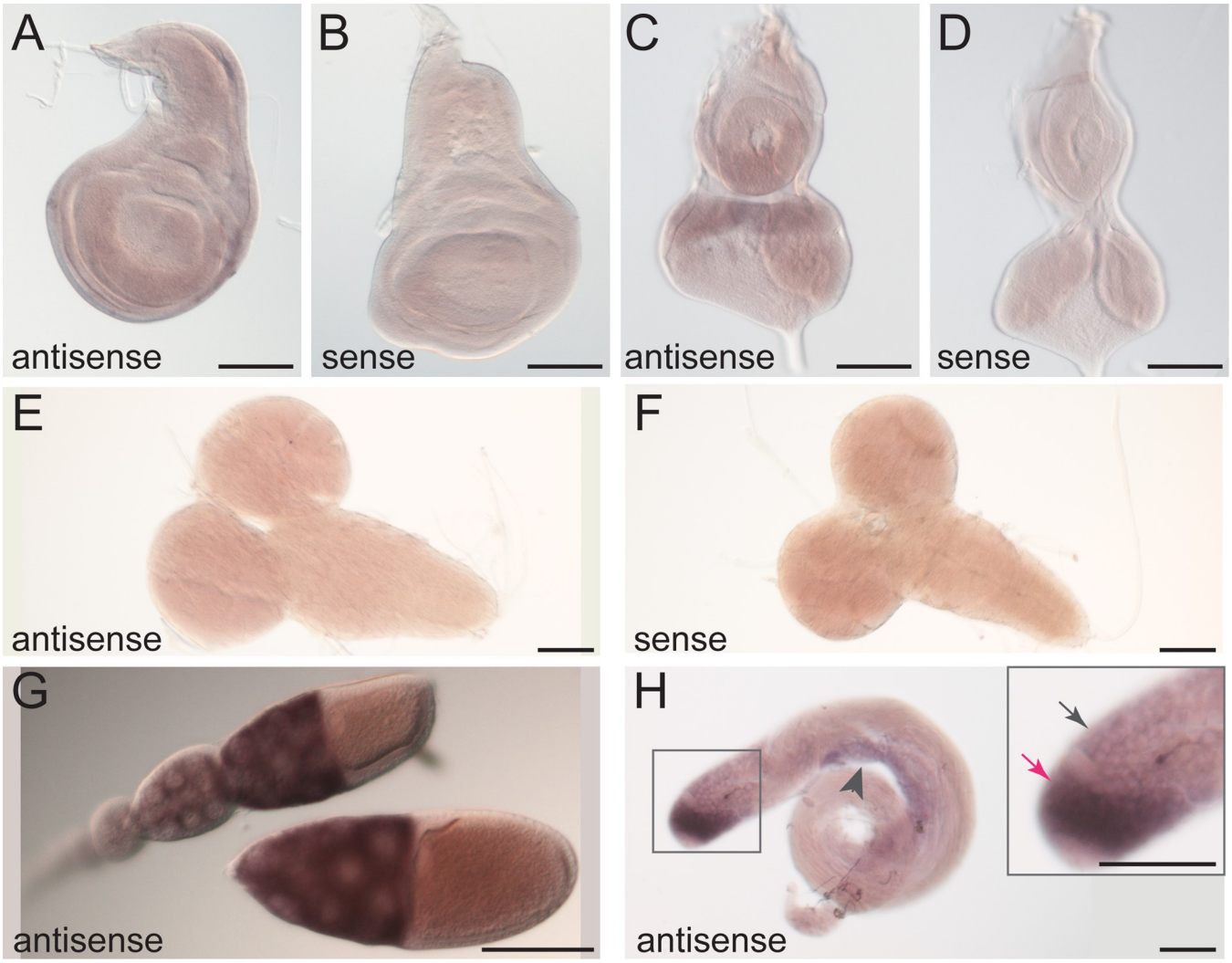

Fig 3. *iPLA$_2$-VIA* mRNA is highly expressed in the adult germline. In situ hybridization to endogenous *iPLA$_2$-VIA* mRNA (purple) in w^{1118} animals shows weak ubiquitous expression in wild-type wing imaginal discs (A) and eye-antennal discs (C). Sense probes (B, D) were used as negative controls. Expression is negligible in larval brains (E, compare to sense probe control in F). Strong expression is seen in both female (G) and male (H) adult germlines. Expression in the male germline (H) is strongest in mitotic spermatogonia (boxed region shown at higher magnification in the inset, magenta arrow indicates spermatogonial region) and moderate in primary spermatocytes (inset, gray arrow) and meiotic spermatids (arrowhead). Scale bars: 100 μm. Positive controls for in situ hybridization are shown in S3 Fig.

https://doi.org/10.1371/journal.pone.0256738.g003

mutants. Surprisingly, *iPLA$_2$-VIA$^{\Delta 23}$* mutant males are fertile, even when they are aged (Fig 4A and 4B).

Loss of function mutations in the enzyme Tafazzin (Taz), a mitochondrially-localized transacylase responsible for most of the CL remodeling activity in cells, lead to male infertility with defects in spermatid individualization in *Drosophila* [23, 51]. Previous results implicated iPLA$_2$-VIA in this pathway, with reduced *iPLA$_2$-VIA* expression compensating for loss of *taz* in male fertility [23]. We therefore closely examined several aspects of spermatogenesis in *taz$^{\Delta 161}$* or *iPLA$_2$-VIA$^{\Delta 23}$* single mutants, as well as in *taz$^{\Delta 161}$ iPLA$_2$-VIA$^{\Delta 23}$* double mutants. In both single mutants and the double mutant, developmentally programmed mitochondrial aggregation is normal in post-meiotic spermatids (Fig 4C–4F), and mitochondrial derivatives begin elongation normally (Fig 4G–4J). At the individualization stage, the actin-rich individualization complexes

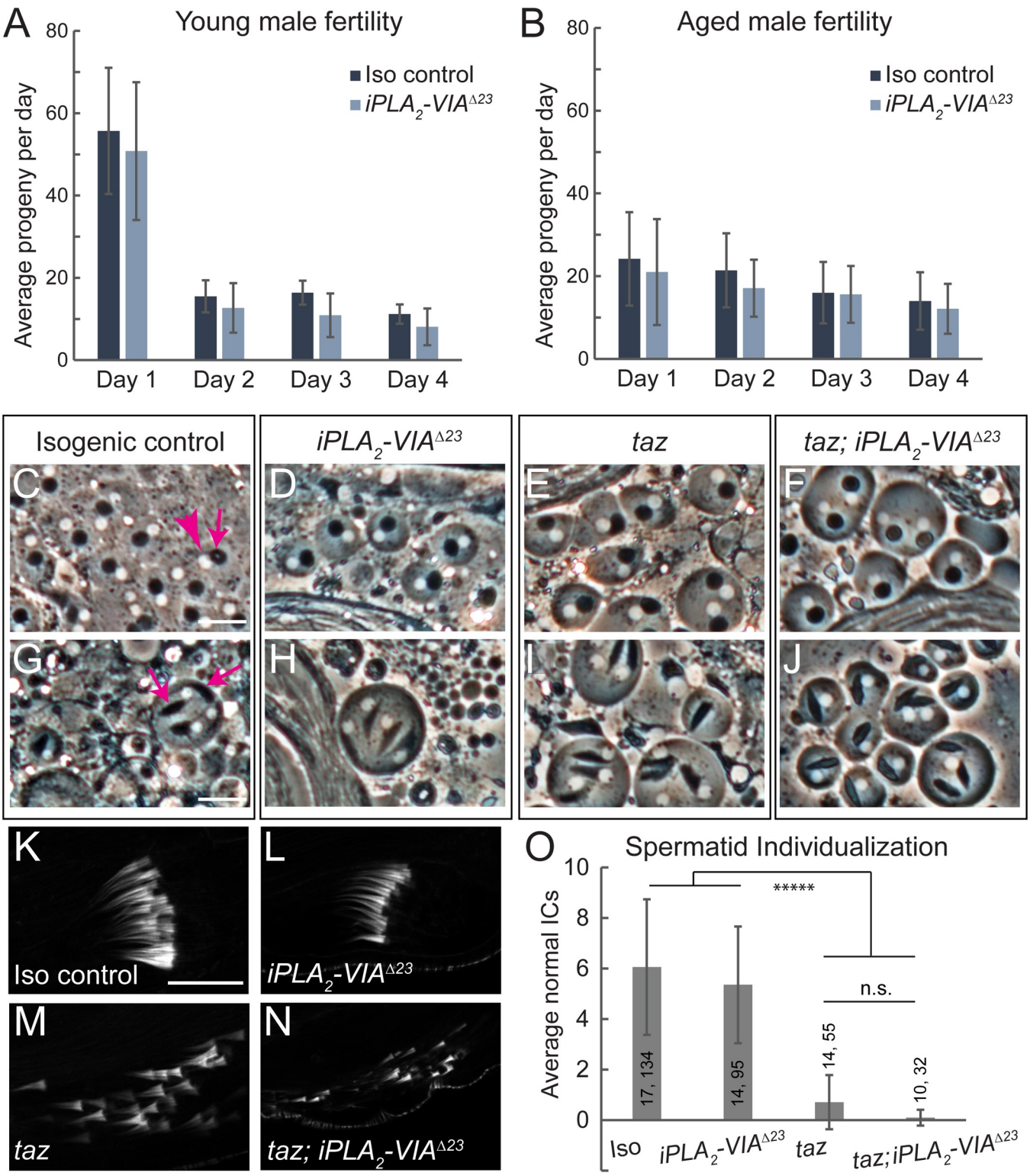

Fig 4. Male fertility and spermatogenesis are normal in *iPLA$_2$-VIA$^{\Delta 23}$* mutants. (A-B) Young (A, 4–5 day old) and aged (B, 20–21 day old) *iPLA$_2$-VIA$^{\Delta 23}$* mutant males (light blue bars) show no fertility defect compared to isogenic controls (dark blue bars). Bars depict average number of adult progeny produced by 10 individual males over the course of four days, error bars represent standard deviation. (C-J) Testis squashes reveal normal post-meiotic mitochondrial Nebenkerne (phase-dark structures, indicated by the magenta arrow in C) in *iPLA$_2$-VIA$^{\Delta 23}$* mutants (D), *taz$^{\Delta 161}$* mutants (E), and *taz$^{\Delta 161}$ iPLA$_2$-VIA$^{\Delta 23}$* double mutants (F), and each Nebenkern is paired with a similarly sized nucleus (phase-light structures, indicated by the magenta arrowhead in C). In slightly later

spermatogenic cysts (G-J), mitochondrial derivatives (indicated by magenta arrows in G) elongate normally in all genotypes. Scale bars: 20 μm. (K-N) Phalloidin staining reveals the individualization complexes (ICs) of the maturing spermatids. In $iPLA_2$-$VIA^{\Delta 23}$ mutants, ICs are normal (L), in contrast with $taz^{\Delta 161}$ mutants, in which ICs are highly disorganized (M). $taz^{\Delta 161}$ $iPLA_2$-$VIA^{\Delta 23}$ double mutants show disorganized ICs (N), like $taz^{\Delta 161}$ single mutants. Scale bar: 20 μm. (O) IC quantification shows no rescue of the $taz^{\Delta 161}$ individualization phenotype by $iPLA_2$-$VIA^{\Delta 23}$ mutation. Number of testes (first number) and number of individualization complexes (second number) quantified for each genotype are indicated on the graph. Bars depict the average number of normal ICs for each genotype, error bars represent standard deviation. Differences assessed by unpaired t-test, $^{*****}p < 10^{-5}$, n.s. indicates not significant.

https://doi.org/10.1371/journal.pone.0256738.g004

(ICs) can be detected by phalloidin staining (Fig 4K, [52]). No IC defects are seen in $iPLA_2$-$VIA^{\Delta 23}$ mutants (Fig 4L). In contrast, ICs are highly disorganized in $taz^{\Delta 161}$ single mutants (Fig 4M, [23]) and in $taz^{\Delta 161}$ $iPLA_2$-$VIA^{\Delta 23}$ double mutants (Fig 4N), with no rescue of the *taz* mutant phenotype by removal of $iPLA_2$-*VIA* (Fig 4O). We also tested the fertility of both $taz^{\Delta 161}$ $iPLA_2$-$VIA^{\Delta 23}$ double mutant males (n = 8) and $taz^{\Delta 161}$ $iPLA_2$-VIA^{EY5103} double mutant males (n = 5) in individual crosses to *yw* females and found both to be completely sterile (0 progeny produced over the course of five days). Therefore, as the $iPLA_2$-*VIA* mutant neither shows similar defects to the *taz* mutant nor rescues it, our data do not support the idea that iPLA$_2$-VIA is a critical unique player in CL remodeling during *Drosophila* spermatogenesis.

Drosophila iPLA$_2$-VIA mutants have reduced female fertility with abnormal mitochondrial aggregation in the germline

Consistent with strong $iPLA_2$-*VIA* expression in the female germline (Fig 3G), there is a significant decrease in female fertility in $iPLA_2$-$VIA^{\Delta 23}$ homozygotes (Fig 5A), and the same effect is seen in hemizygotes, supporting the locus-specificity of the phenotype (Fig 5B). This is accompanied by a decrease in number of eggs laid (Fig 5C and 5D) but not maternal lethality in embryos or larvae (S4 Fig), suggesting that $iPLA_2$-*VIA* is necessary before fertilization, during oogenesis. Although major developmental defects are not evident in $iPLA_2$-$VIA^{\Delta 23}$ mutant ovaries, we observe striking mitochondrial aggregation in the germlines of aged mutant females. The mitochondrially targeted fluorescent reporter transgene *Psqh-mito-EYFP*, which consists of YFP fused to the mitochondrial localization signal of human cytochrome c oxidase 8A, decorates a diffuse mitochondrial network in the nurse cells of young females, in both null mutants and controls (Fig 6A and 6B). By three weeks of age, mitochondria aggregate abnormally in the mutant, despite maintaining their normal diffuse distribution in background control and heterozygous genotypes (Fig 6C and 6D). Aggregation is especially noticeable in mid-oogenesis stages 8–9. In younger egg chambers, mitochondria are less diffuse even in control genotypes, making the mutant phenotype harder to distinguish (for example, see Fig 7A'). To quantify mitochondrial aggregation, we used ImageJ to outline the mito-YFP signal areas. In egg chambers with a normal diffuse mitochondrial network, the outlined mito-YFP signal is extensive and complex, but in egg chambers with aggregated mitochondria, the outlines separating areas of signal from background are sparser (Fig 6E and 6F). Taking the raw integrated density of the mito-YFP outlines in the area of the nurse cells in ImageJ reveals a highly significant quantitative reduction in the intricacy of the mito-YFP network in mutant germlines at mid-oogenesis compared to controls, in females three weeks of age and older (Fig 6G and 6H). Although $iPLA_2$-$VIA^{\Delta 23}$ mutant flies do not survive to six weeks of age [26, 36, 39], neither control genotype nor mito-YFP stock homozygotes show mitochondrial aggregation even at this late age (Figs 6I and S5A and S5B).

Because mitochondrial aggregation can be a sign of damage [53, 54], we examined mitochondrial potential in mitochondrial preparations from lysed ovaries using the potential-sensitive fluorescent dye JC-1. Aged $iPLA_2$-$VIA^{\Delta 23}$ mutant ovaries have reduced JC-1 fluorescence compared to controls, indicating loss of mitochondrial potential (Fig 6J). By five weeks of age,

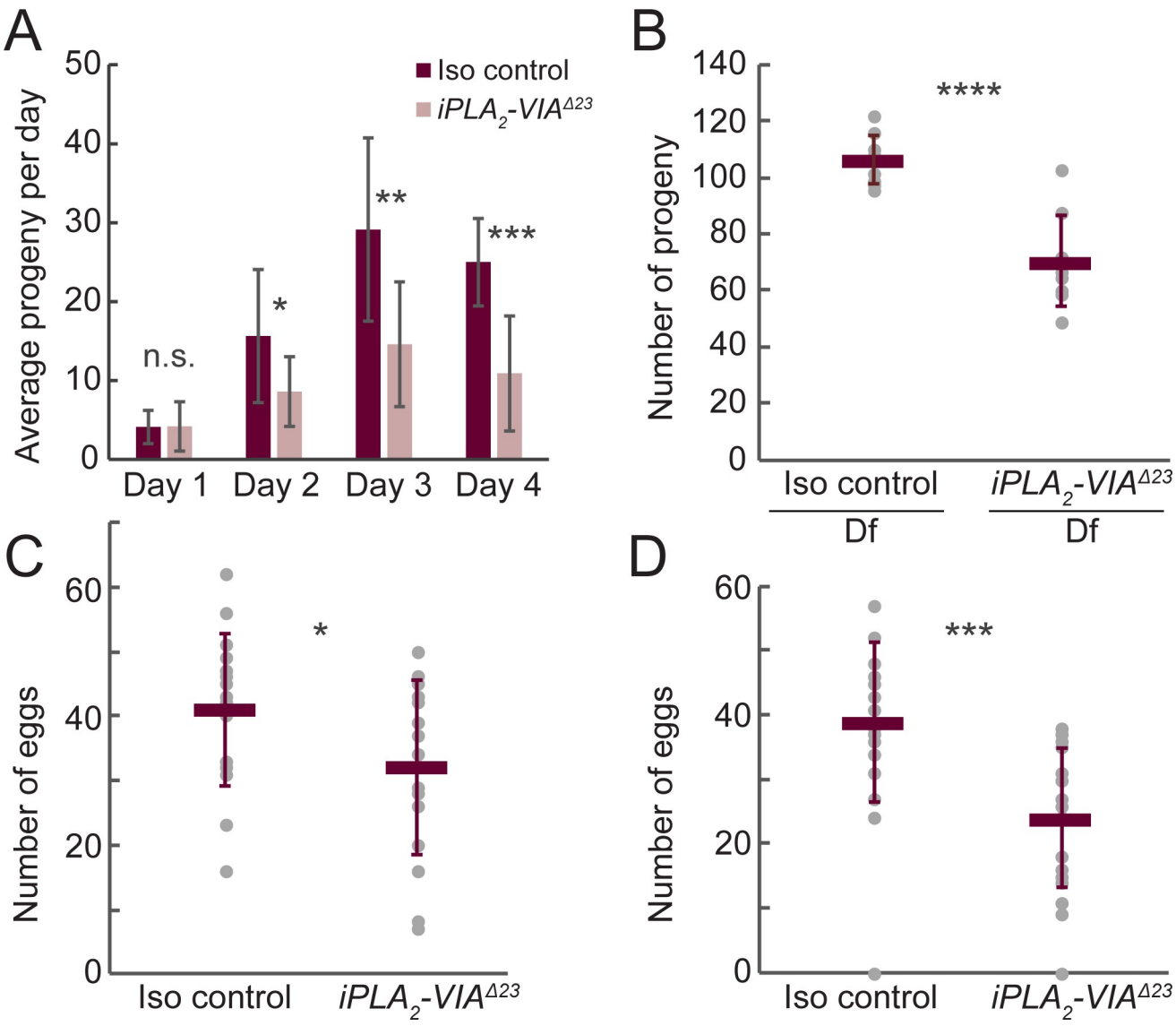

Fig 5. Female fertility is reduced in *iPLA$_2$-VIA$^{\Delta 23}$* mutants. (A) Young (<1 week old) *iPLA$_2$-VIA$^{\Delta 23}$* homozygous mutant females (light pink bars) produce fewer adult progeny compared to isogenic controls (dark red bars). Bars depict average number of adult progeny produced by 10 individual females over the course of four days, error bars represent standard deviations. (B) Hemizygous mutant females (*iPLA$_2$-VIA$^{\Delta 23}$/Df(3L)BSC282)* produce fewer adult progeny compared to isogenic controls. Dark red bars represent average number of adult progeny produced by 10 individual females over the course of four days, error bars are standard deviations. (C-D) Egg laying by *iPLA$_2$-VIA$^{\Delta 23}$* mutants is reduced compared to isogenic controls in young (C, one week old) and aged (D, 18–19 day old) females. Dark red bars represent average number of eggs produced by 20 individual females over the course of four days, error bars are standard deviations. Differences assessed by unpaired t-test, n.s. not significant, $^{*}p < 0.1$, $^{**}p < 0.02$, $^{***}p < 0.001$, $^{****}p < 0.0001$.

https://doi.org/10.1371/journal.pone.0256738.g005

germ cells of the mutant undergo apoptosis, with fragmented nuclei and cleaved caspase-3 staining, in contrast to controls (Fig 6K–6M).

To confirm further that mitochondrial aggregation is independent of the mito-YFP transgene, we examined another mitochondrial marker, immunofluorescence for the ATP-5A protein. We again saw mitochondrial aggregation in germ cells from aged *iPLA$_2$-VIA$^{\Delta 23}$* mutant females and not in those from isogenic control flies (S5C and S5D Fig), but we were not able to quantify it due to the variability of the staining. We noticed, though, that on average germ cells from aged *iPLA$_2$-VIA$^{\Delta 23}$* mutant females have lower ATP-5A signal intensity than those from

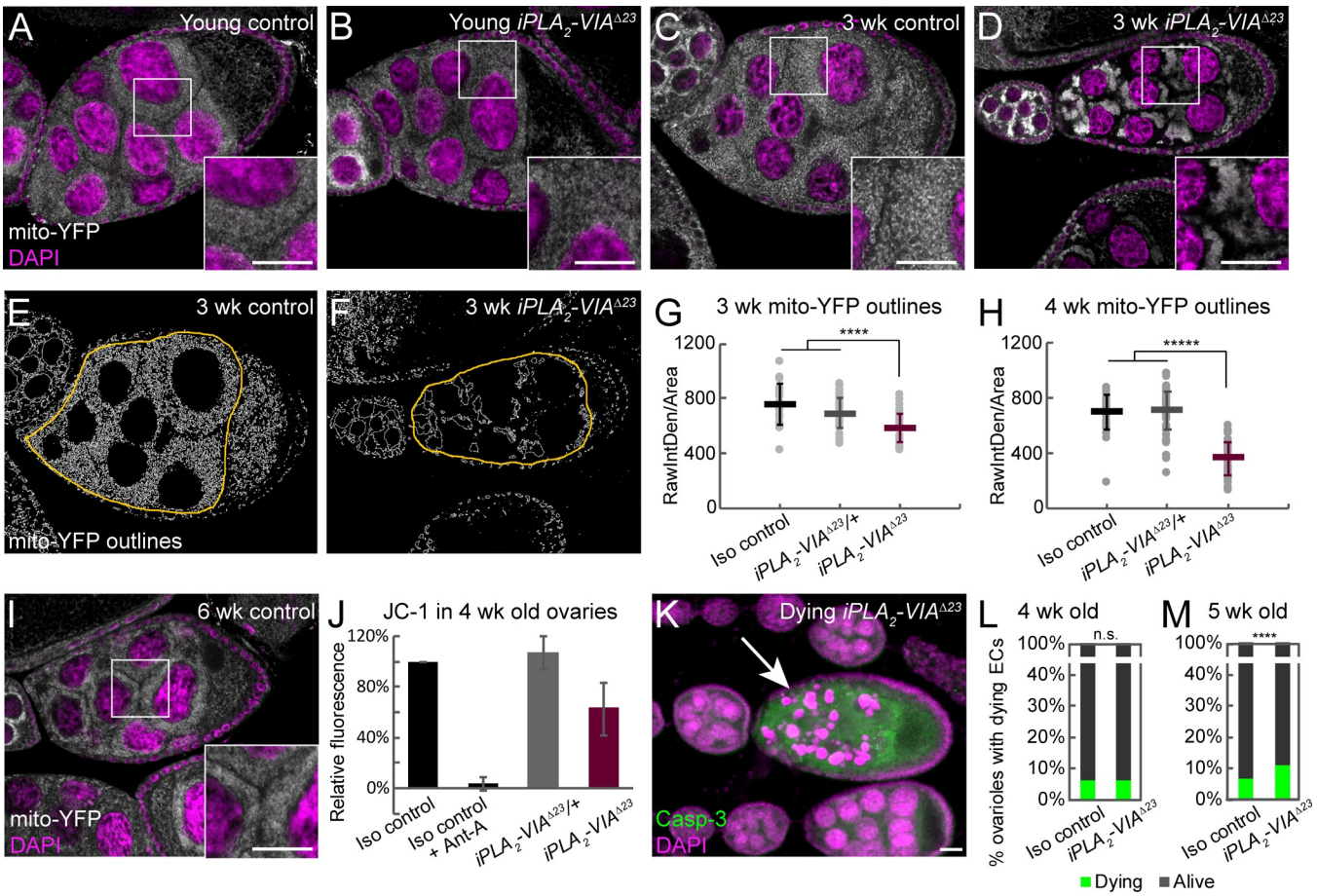

Fig 6. Germ cells from *iPLA2-VIA$^{\Delta 23}$* mutant females have abnormal mitochondrial distribution, reduced mitochondrial potential, and elevated apoptosis. (A-B) *Psqh-mito-EYFP* (white) was used to observe the mitochondrial distribution in female germ cells from young (<1 week old) *iPLA$_2$-VIA$^{\Delta 23}$* mutants (*Psqh-mito-EYFP*, *iPLA$_2$-VIA$^{\Delta 23}$/iPLA$_2$-VIA$^{\Delta 23}$*) and heterozygous controls (*Psqh-mito-EYFP*, *iPLA$_2$-VIA$^{\Delta 23}$/revertantΔ11*). Nuclei are stained with DAPI (magenta). Magnified views of the boxed regions are shown in the insets. (C-D) Mito-YFP labeled mitochondria appear clumpy in germ cells from aged (3 week old) *iPLA$_2$-VIA$^{\Delta 23}$* female flies (D) but not controls (C, *Psqh-mito-EYFP/revertantΔ11*; for *Psqh-mito-EYFP*, *iPLA$_2$-VIA$^{\Delta 23}$/revertantΔ11* heterozygotes see quantification in G and H). (E-H) Mito-YFP signal within the area of the germline nurse cells was outlined using ImageJ (white in E-F, yellow delimiting outlines indicate region of interest, i.e., the nurse cells) and the raw integrated density of the mito-YFP outline signal was used to quantify clumpiness (G-H). Homozygous *iPLA$_2$-VIA$^{\Delta 23}$* mutants (dark red, *Psqh-mito-EYFP*, *iPLA$_2$-VIA$^{\Delta 23}$/iPLA$_2$-VIA$^{\Delta 23}$*, n = 39) show significantly reduced mito-YFP outline signal compared to heterozygotes (gray, *Psqh-mito-EYFP*, *iPLA$_2$-VIA$^{\Delta 23}$/revertantΔ11*, n = 43) and isogenic controls (black, *Psqh-mito-EYFP/revertantΔ11*, n = 19) at 3 weeks (G) and 4 weeks old (H; black, *Psqh-mito-EYFP/revertantΔ11*, n = 42; gray, *Psqh-mito-EYFP*, *iPLA$_2$-VIA$^{\Delta 23}$/revertantΔ11*, n = 67; dark red, *Psqh-mito-EYFP*, *iPLA$_2$-VIA$^{\Delta 23}$/iPLA$_2$-VIA$^{\Delta 23}$*, n = 50), indicating increased clumpiness. Bars represent averages and standard deviations for each condition. Differences assessed by unpaired t-test, $^{****}p < 0.0001$, $^{*****}p < 10^{-6}$. (I) Controls (*Psqh-mito-EYFP/revertantΔ11*) do not show mito-YFP clumpiness even at 6 weeks of age, while *iPLA$_2$-VIA$^{\Delta 23}$* mutant females do not survive to 6 weeks. (J) Ovaries from 4 week old *iPLA$_2$-VIA$^{\Delta 23}$* females (dark red bar) show reduced JC-1 fluorescence compared to age matched controls (black, *Psqh-mito-EYFP/revertantΔ11;* gray, *Psqh-mito-EYFP*, *iPLA$_2$-VIA$^{\Delta 23}$/revertantΔ11*) using plate-based fluorimetry. In each experiment, the red (595 nm) JC-1 fluorescence of the heterozygote or the mutant is expressed as a percentage of the fluorescence of the control, and 3–4 biological replicates are averaged. Error bars are standard deviations. Antimycin A was used as a mitochondrial poison to demonstrate the specificity of the JC-1 signal. (K) By 5 weeks of age, *iPLA$_2$-VIA$^{\Delta 23}$* mutants show increased levels of germline apoptosis, marked by cleaved caspase-3 staining (green) and fragmentation of the nurse cell nuclei (DAPI, magenta), quantified in M. (L-M) The percentage of ovarioles containing dying egg chambers (green bars) is elevated in *iPLA$_2$-VIA$^{\Delta 23}$* mutants compared to isogenic controls at 5 weeks of age (M, >1300 ovarioles counted for each genotype across four biological replicates) but not 4 weeks (L, >900 ovarioles counted for each genotype across three biological replicates). Dying egg chambers were identified by their fragmented nurse cell nuclei and cleaved caspase-3 staining, as shown in (K). Statistical comparison by two proportion z-test, n.s. not significant, $^{****}p < 0.0001$. Scale bars: 20 μm.

https://doi.org/10.1371/journal.pone.0256738.g006

control flies (S5E and S5F Fig), which might indicate that damaged mitochondria in the mutant are subject to quality control mechanisms involving degradation. This might be specific to the endogenous respiratory complex proteins, including ATP-5A, as the mito-YFP marker does not show this lowered signal in the mutant.

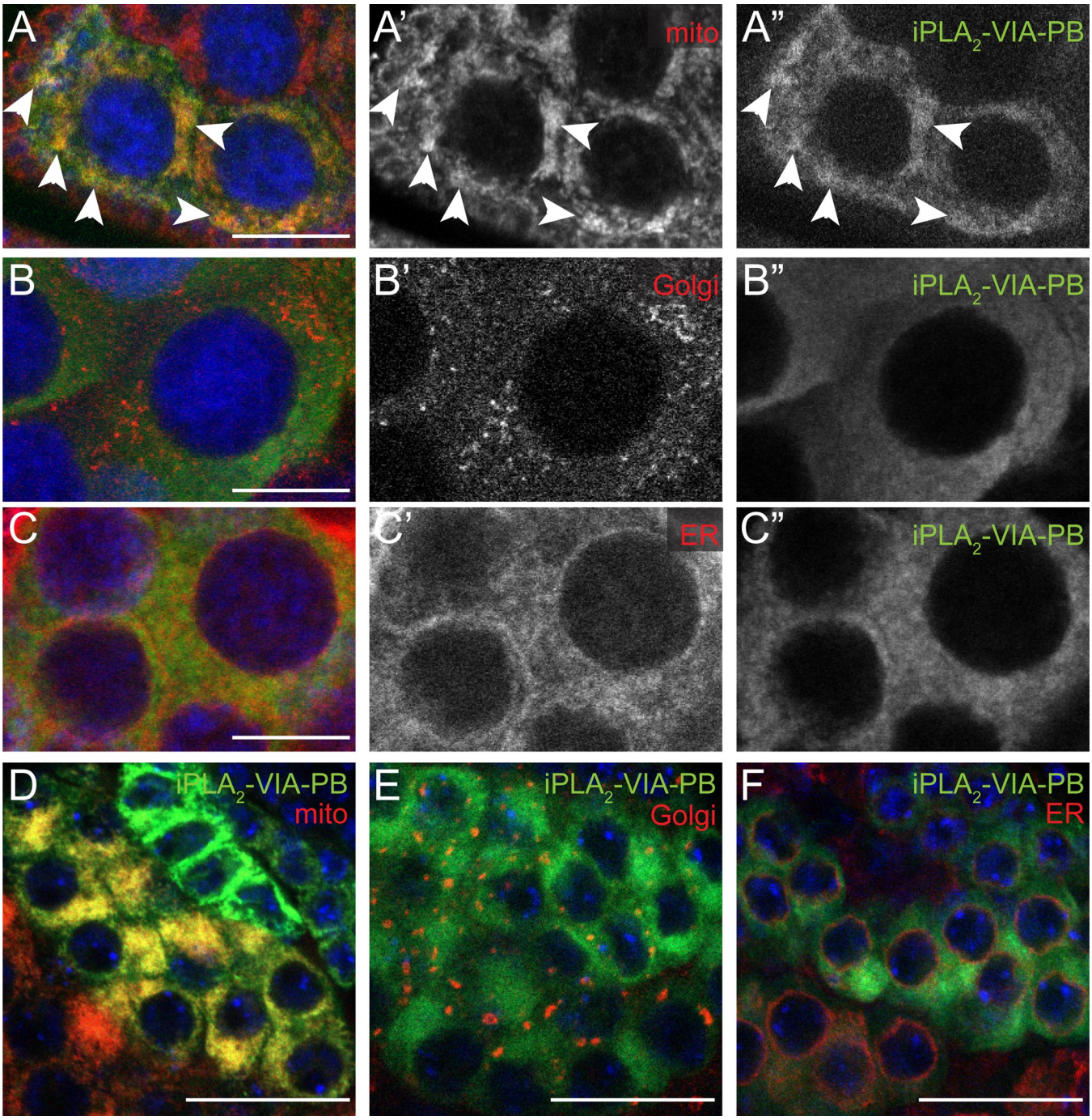

Fig 7. iPLA$_2$-VIA-PB protein localizes to mitochondria in female and male germ cells. (A-C) In the female germline, HA-tagged wild-type iPLA$_2$-VIA-PB (green, grayscale shown in A"-C", expressed with *NGT40-GAL4*) strongly colocalizes with a mitochondrial marker (A, red, *Psqh-mito-EYFP*, arrowheads) and shows minimal colocalization with Golgi (B, red, anti-Golgin 84) and ER (C, red, anti-Calnexin 99A) markers. Individual channels for mitochondria, Golgi, and ER shown in A', B', C', respectively. (D-F) In male germ cells, iPLA$_2$VIA-PB (green, expressed with *bam-GAL4-VP16*) also colocalizes more strongly with a mitochondrial marker (D, red, *UAS-mCherry-mitoOMM*) than Golgi (E, red) or ER (F, red) markers. Scale bars: 20 μm.

https://doi.org/10.1371/journal.pone.0256738.g007

iPLA$_2$-VIA-PB localizes to mitochondria in germ cells

Because iPLA$_2$-VIA has been implicated in numerous different activities in a variety of cellular compartments, we examined the subcellular localization of our HA-tagged wild-type *UAS-*

iPLA$_2$-VIA-PB transgene, which can rescue the climbing defect of the mutant (Fig 2C and 2D). Following expression in female germ cells with *NGT40-GAL4*, the wild-type transgene colocalizes most strongly with a mitochondrial marker (Fig 7A–7C), consistent with the mitochondrial defect in the mutant. The transgene also colocalizes strongly with a mitochondrial marker in male germ cells, when expressed using *bam-GAL4* (Fig 7D–7F). We additionally examined localization in somatic cells using the *tubulin-GAL4* driver and the large polyploid cells of the larval fat body and salivary gland [55]. Interestingly, colocalization in these tissues is strongest with a Golgi marker (S6A and S6D Fig), suggesting that subcellular localization of iPLA$_2$-VIA is regulated differently in distinct cell types and possibly is correlated with function.

Discussion

iPLA$_2$-VIA in phospholipid metabolism

Tight regulation of iPLA$_2$-VIA levels and activity is important for cell cycle dependent phospholipid accumulation [56] and PC homeostasis [40, 41] in several mammalian cultured cell lines. However, genetic perturbation of the rate-limiting PC synthesis enzyme Pcyt1 in whole flies does not cause obvious changes in *iPLA$_2$-VIA* mRNA expression (S1 Fig), nor do we find evidence of genetic interactions between *iPLA$_2$-VIA* and *pcyt1* in viability or fertility (Table 2). To our knowledge, this is the first report on a possible genetic interaction between *iPLA$_2$-VIA* and *pcyt1* in an intact organism. *iPLA$_2$-VIA* also shows no genetic redundancy for viability with *sws/NTE*, a conserved paralog important for PC homeostasis (Table 3, [43]). We see no global downregulation of *iPLA$_2$-VIA* mRNA in an *eas* mutant with reduced PE levels either (S1 Fig, [57]). *iPLA$_2$-VIA* mRNA expression is very low in wild-type imaginal discs (Fig 3), despite substantial cell proliferation there [58], and *iPLA$_2$-VIA* null mutants are developmentally viable (Table 1). Altogether, our data suggest that iPLA$_2$-VIA does not play unique roles in phospholipid accumulation in *Drosophila*, consistent with recent mass spectrometry analysis of another *iPLA$_2$-VIA* knockout mutant [39].

iPLA$_2$-VIA in male fertility and CL remodeling

We expected that, like the mouse ortholog, *Drosophila* iPLA$_2$-VIA would be important for male fertility, in accord with its high expression in the male germline (Fig 3, [38]). Furthermore, it was reported to interact genetically with the mitochondrially-localized CL remodeling enzyme Taz in *Drosophila* male fertility [23]. We observed iPLA$_2$-VIA colocalization with mitochondria in male germ cells (Fig 7), as has been documented in cultured mammalian cells [19, 21]. Surprisingly, however, *iPLA$_2$-VIA* mutant males are fully fertile, with normal spermatid mitochondrial morphogenesis and, unlike the *taz* mutant, normal spermatid individualization (Fig 4). Moreover, we find no evidence that *iPLA$_2$-VIA* loss of function mutations interact genetically with *taz*, in contrast to a prior report [23]. Our genetic data in the testis therefore may argue against the idea that iPLA$_2$-VIA is a major unique player in CL remodeling. This is consistent with mass spectrometry results showing minimal CL changes in *iPLA$_2$-VIA* hypomorphic mutant heads or whole flies [26, 30] and with recent studies indicating that Taz can remodel CL independently of phospholipases [59].

iPLA$_2$-VIA in female fertility

iPLA$_2$-VIA mRNA is highly expressed in the wild-type female germline (Fig 3), and *iPLA$_2$-VIA* mutant females have reduced fertility compared to controls (Fig 5). Despite normal ovariole morphology, germ cells in aged *iPLA$_2$-VIA* mutant females have abnormally aggregated

mitochondria with decreased membrane potential, and they eventually die by apoptosis (Fig 6). In HeLa cells, pharmacological disruption of mitochondrial membrane potential induces aggregation via stabilization of the mitochondrially targeted kinase PINK1 and recruitment of its substrate and partner Parkin, an E3 ubiquitin ligase. Ubiquitinated Parkin substrates on the outer mitochondrial surface recruit the autophagy receptor p62/SQSTM1, which promotes aggregation, possibly for sequestration before degradation by mitophagy [53, 54]. Intriguingly, mitochondrial aggregation in *Drosophila* female germ cells has been observed in *pink1* and *parkin* mutants, similarly to *iPLA$_2$-VIA* mutants [60, 61]. This might suggest a parallel mechanism for mitochondrial damage detection and aggregation, independent of the PINK1-Parkin pathway, that perhaps relies on another mitophagy receptor, for example BNIP3, which is known to be active in the female germline [62, 63]. It is tempting to propose that in the absence of iPLA$_2$-VIA, PINK1, or Parkin, mitochondrial damage accumulates and leads to aggregation. Eventually, persistent mitochondrial damage may overwhelm cytoprotective mechanisms like aggregation and mitophagy, leading to apoptosis. We thus hypothesize that iPLA$_2$-VIA protects germline mitochondria from accumulated injury that can result in apoptosis, as in other contexts [19, 22, 25]. A direct effect is supported by the localization of iPLA$_2$-VIA to mitochondria in germ cells (Fig 7). Reduced mitochondrial membrane potential also has been observed in brains of an *iPLA$_2$-VIA* hypomorph [26], possibly suggesting a mechanistic connection between the germline and neuronal phenotypes.

iPLA$_2$-VIA in neuromuscular degeneration

Our *iPLA$_2$-VIA* mutants show a severe decline in locomotor ability with age, like other *Drosophila* and mouse mutant models (Fig 2, [26, 36, 64–67]). Phenocopy by RNAi knockdown in neurons is consistent with the idea that iPLA$_2$-VIA acts autonomously to protect against neurodegeneration [26, 36]. Our data suggest that iPLA$_2$-VIA also is important in other tissues to prevent locomotor decline, notably muscle, in accord with a report of muscle degeneration in two human PLAN patients [68]. The strength of the phenocopy with muscle-specific knockdown is comparable to that seen for *pink1* (Fig 2). *PINK1* and its partner *parkin* are well-established disease loci for autosomal recessive parkinsonism in humans [10]. As discussed above, PINK1 accumulates on the outer mitochondrial membrane under stress conditions and recruits Parkin to activate quality control mechanisms, including mitophagy, that maintain the overall integrity of the cellular mitochondrial network [69]. In their absence, accumulation of damaged mitochondria leads to degeneration of neurons, as well as muscle in *Drosophila* [48, 49]. The parkinsonism in human patients, as well as the locomotor defects and germline mitochondrial aggregation in flies, suggest some similarities between loss of *iPLA$_2$-VIA* and loss of *pink1* or *parkin* [60, 61]. Notably, however, *Drosophila pink1* and *parkin* mutants display locomotor defects at earlier time points, as well as other indications of muscle degeneration, including crushed thoraces and wing posture abnormalities, not seen in *iPLA$_2$-VIA* mutants [48, 49]. Additionally, the normal fertility and spermatid mitochondrial morphology in *iPLA$_2$-VIA* mutant males stand in contrast to the highly penetrant male germline defects of *pink1* and *parkin* mutants [48, 49, 70].

Although many studies have implicated iPLA$_2$-VIA in mitochondrial maintenance via catalytic removal of damaged phospholipid acyl chains, our data show that a transgene with a serine-to-alanine mutation in the catalytic site can rescue the climbing defect of the mutant, consistent with another report in which a human iPLA$_2$-VIA transgene carrying the analogous catalytic site mutation rescued bang-sensitivity and lifespan defects of *iPLA$_2$-VIA* mutants [39]. This suggests that phospholipase activity is not the only important aspect in iPLA$_2$-VIA mediated cytoprotection, possibly explaining the observation that mutations associated with *PLA2G6*-associated dystonia-parkinsonism do not disrupt catalytic activity [47]. iPLA$_2$-VIA's non-catalytic activities

remain to be characterized and might depend on its ankyrin motifs, which are predicted to mediate protein-protein interactions [32]. Moreover, while loss of iPLA$_2$-VIA is associated with aberrant mitochondrial morphology in neurons, it also is accompanied by defects in numerous other processes, including Ca^{+2} homeostasis, ER membrane equilibrium, and vesicle trafficking [26–28, 34, 39]. Thus, as with other forms of neurodegeneration, further investigation is necessary to determine which defects are drivers and which are passengers in PLAN.

Materials and methods

Drosophila strains

Drosophila were raised on standard media at 23˚C. *yw (BDSC_6599)*, *P[EPgy2]iPLA2-VIA^{EY5103} (BDSC_15947)*, *Df(3L)BSC394 (BDSC_24418)*, *Df(3L)BSC282 (BDSC_23667)*, *pcyt1^{16919} (BDSC_7319)*, *sws^{4} (BDSC_28121)*, *HMS01544 (BDSC_36129)*, *UAS-mCherry-mitoOMM (BDSC_66532* and *BDSC_66533)*, *Psqh-mito-EYFP (BDSC_7194)*, *DJ667-GAL4 (BDSC_8171)*, and *pink1-RNAi (HMS02204*, *BDSC_41671)* were from Bloomington *Drosophila* Stock Center; *P[GSV6]GS15374* (*DGGR_206187*) was from Kyoto *Drosophila* Genomics and Genetic Resource Center; *tubulin-GAL4* and *elav-GAL4* were gifts from J. Treisman; *bam-GAL4-VP16* was a gift from Y. Yamashita; *NGT40-GAL4* was a gift from R. Lehmann; *eas^{KO}* and isogenic controls were gifts from the Jan lab [44]; *taz$^{\Delta 161}$* mutants were a gift from M. Schlame and M. Ren [71].

The *iPLA$_2$-VIA$^{\Delta 23}$* mutant was generated by excision of the P element EY5103, which is marked with mini-w+. The location of EY5103 was confirmed by inverse PCR before excision. Over 450 w- lines were screened for lesions in the region of interest by PCR with primers flanking the insertion site (F: 5′-CCGTGCTCTGTGGAATCAGT-3′, R: 5′-GCGCCAAAGCTAGAATTCCG-3′). Mutant line Δ23 was identified in the PCR screen, and the genomic region of *iPLA$_2$-VIA* was sequenced to confirm the lesion. Several precise excision lines from the screen were kept as isogenic controls and confirmed by sequencing to be wild-type in the *iPLA$_2$-VIA* gene region. This sequencing also confirmed that the same polymorphisms were present in the Δ23 line and the precise excision lines. Revertant line Δ11 was used as the isogenic control in all experiments described here. All recombinant chromosomes made with the *iPLA$_2$-VIA$^{\Delta 23}$* allele were confirmed by PCR.

RT-PCR

Whole fly RNA was prepared from mixed sex samples (5–15 flies per sample, flies < 1 week old) with Trizol reagent (Invitrogen) according the manufacturer's protocol. RNA preparations were treated with DNase I to remove genomic DNA (New England Biolabs) and quantified using NanoDrop (ThermoFisher). cDNAs were reverse transcribed using Superscript III (Invitrogen) according to the manufacturer's protocol, from an equal mass of RNA for each sample per experiment (1–1.5 μg).

Qualitative PCRs were 25 cycles, unless noted otherwise. Experimental (*iPLA$_2$-VIA*) and control primers (*actin*) were included in the same tube to control for pipetting. All experiments were repeated in triplicate. Quantifications were performed using Bio-Rad ImageLab 5.0. PCR primers were as follows:

Gene	Forward primer	Reverse Primer
iPLA$_2$-VIA	5′-CGACCCACCTCGGATTCC-3′	5′-GACCACCAGACATTGGACG-3′
actin	5′-CCATCAGCCAGCAGTCGTCTAATC-3′	5′-GGTTGGCCTTGGGGTTCAGC-3′
pcyt1	5′-TCAATGGCGAAAGCACTCGT-3′	5′-CGAATCGCGGGTATCTGGA-3′

Quantitative PCRs were performed on cDNA samples diluted 6x, using SYBR green + regular ROX mix (MCLab, HSM-400). Reactions were run on an Applied Biosystems 7300 Real-Time PCR System. Primers were:

Gene	Forward primer	Reverse Primer
iPLA$_2$-VIA	5´-CGGCCCTATAACAGCGAGTT-3′	5´-AAATGTCACTGGCGCTCGTA-3′
rp49	5′-CCAAGCACTTCATCCGCCACC-3′	5′-GCGGGTGCGCTTGTTCGATCC-3′

Climbing assays

Climbing tests were performed as in [72]. Groups of 6–13 male or female flies were tapped to the bottom of a fresh food vial and given 20 s to climb 6 cm, into a new empty vial placed on top of the old one. Each group was given five climbing trials per assay. Each fly in the group was given one point for every success, and the total number of points for the group was divided by the number of flies in the group to yield the climbing index. Climbing indices were averaged for at least 6 groups per condition and plotted with standard deviations. Climbing indices for each condition were verified for normal distribution around the average. Statistical comparisons by unpaired t-tests.

Transgene generation

The wild-type iPLA$_2$-VIA-PB transgene was generated by PCR from publicly available iPLA$_2$-VIA cDNA (https://dgrc.bio.indiana.edu/, clone RE23733) using Platinum *Pfx* polymerase (Life Technologies, 11708013) and cloned into pUASg-HA.attB (http://www.flyc31.org/) or pPWH (https://dgrc.bio.indiana.edu/vectors/Catalog?product_category=3) using the Gateway system (Life Technologies). PCR primers were: 5′-(CACC)ATGGCGTGGATGGCGTTAG-3′ and 5′-AATCCGTCTTGCATGCGATTTTAG-3′. To introduce the serine-to-alanine mutation, an upstream PCR product was generated with primers 5′-TCTGTACCGGTCGCCG GTG-3′ and 5′-TAGAATTCCGCCAGTAGCGGTGCCGG-3′, and a downstream PCR product was generated with primers 5′-ATTGCCGGCACCGCTACTGGCGGAATT-3′ and 5′-CA TGGCGTCTAGAGTCGGGTTGT-3′. The upstream and downstream PCR products were annealed and used as template to generate a PCR product spanning the entire segment. The mutated segment was cloned to replace the corresponding wild-type segment using the unique SgrA1 and Xba1 restriction sites. PCR products were cleaned with QIAquick PCR Purification kit (Qiagen 28104), digested DNA was cleaned with QIAquick Gel Extraction kit (Qiagen 28704), and plasmid DNA was prepared with QIAprep Spin Miniprep kit (Qiagen 27104) and Qiagen Plasmid Midi kit (Qiagen 12143). All constructs were verified by sequencing (Eton Bioscience) before injecting into flies (Genetivision). The VK37 ΦC31 landing site was used for both *UAS-iPLA$_2$-VIA-PB WT* and *UAS-iPLA$_2$-VIA-PB SA*.

RNA in situ hybridizations

iPLA$_2$-VIA cDNA plasmid (https://dgrc.bio.indiana.edu/, clone RE23733) was linearized with BamH1 (sense) or Not1 (antisense) restriction digest, and digoxigenin-labeled RNA probes were transcribed using a digoxigenin-UTP in vitro transcription labeling mix (Roche) and either T7 or T3 RNA polymerase (Roche). Probe was carbonate-treated to reduce size. Control probes (S3 Fig) for *wg* and *cycB* were transcribed similarly, from PCR products made from genomic DNA. The PCR primers were: 5′-CAGGAATTCGACGGGAACCA-3′ and 5′-TAAT

ACGACTCACTATAGGGAGAGTGCGTTTGGTGTCCTTGAC-3′ for *cycB*; 5′-GTGAAGTG CAAGCTGTGTCG-3′ and 5′-TAATACGACTCACTATAGGGAGAAAACGACAGCATGAG GAGGG-3′ for *wg*.

For imaginal discs, protocol was adapted from [73]. Third instar larvae were dissected in PBS and fixed in 4% formaldehyde/PBT (PBT is PBS/0.1% Tween-20) for 1 h at 4˚C. Tissues were washed once in 50% PBT:methanol and once in 100% methanol before overnight storage in 100% methanol at -20˚C. After two ethanol washes, tissues were incubated in 1:1 xylenes:ethanol for 1 h at 4˚C. Tissues were washed again twice in ethanol and once in 50% methanol, and then incubated in 80% acetone for 10 min at -20˚C. Tissues were washed twice in PBT and re-fixed in 4% formaldehyde/PBT for 20 min at 4˚C. After three PBT washes, tissues were equilibrated into hybridization buffer and hybridized overnight at 65˚C with digoxigenin-labeled RNA probes. The next day, tissues were equilibrated back into PBT, washed extensively, and incubated with alkaline phosphatase conjugated anti-digoxigenin antibody (1:1000, Roche) for 1 h at room temperature. After several PBT washes, tissues were washed in AP buffer and color was developed using NBT and BCIP substrates. Hybridization and color development were performed as in [74]. Larval and imaginal tissues were mounted in 80% glycerol.

For ovaries, protocol was performed as in [74].

For testes, protocol was performed as in [75]. Stained testes were mounted in 60% glycerol: PBS.

Tissue staining and immunofluorescence

For phalloidin staining, testes were dissected in PBS and fixed in 5% formaldehyde/PBX (PBS/0.1% Triton X-100) for 20 min at room temperature, washed in PBX for 15–20 min, and stained with rhodamine-phalloidin (1:200, Sigma-Aldrich) and DAPI (1:4000, Roche) for 20 min at room temperature. Following three washes in PBX, tissues were mounted in Fluoromount G (Southern Biotechnology).

For antibody staining, testes were fixed and washed as above. Testes were blocked in PBS + 5% normal donkey serum (Jackson ImmunoResearch) + 1% Triton X-100 before the primary antibody incubation. Primary antibody incubations were performed overnight (in PBX + 5–10% normal donkey serum) at 4˚C, washed three times in PBX, and incubated with secondary antibodies, DAPI, and rhodamine-phalloidin for 2 hours at room temperature.

Larvae were dissected in PBS and fixed in 4% formaldehyde for 30 min at 4˚C. Tissues were blocked in PBS + 5% normal donkey serum before the primary antibody incubation. For ovary antibody staining, adult females were mated to males on live yeast paste for 1–2 days before dissections. Ovaries were dissected in PBS and combed open, fixed in 5% formaldehyde for 13 min at room temperature, rinsed in PBX, washed 3–4 times in PBX, and blocked in PBS + 5% normal donkey serum + 1% Triton X-100 before primary antibody incubation. Antibody incubations were performed as above.

Primary antibodies used were mouse anti-ATP-5A (1:1000, Abcam, ab14748), mouse anti-Calnexin 99A (1:2, Developmental Studies Hybridoma Bank, ER marker), mouse anti-Golgin 84 (1:2, Developmental Studies Hybridoma Bank, Golgi marker), rat anti-HA (1:100, Roche, 3F10), rabbit anti-cleaved caspase 3 (1:100, Cell Signaling Technology, 9664), and rabbit anti-GFP (1:5000, Life Technologies, A6455). Secondary antibodies were Alexa Fluor® 488-AffiniPure Donkey Anti-Rat or Anti-Rabbit IgG and Cy3-AffiniPure Donkey Anti-Mouse IgG or Anti-Rat IgG (1:200, Jackson ImmunoResearch).

Images were captured using an Olympus IX-81 motorized inverted microscope with XM-10 monochrome camera (lenses: 10x/0.3 NA, 20x/0.75 NA, 40x oil/1.3 NA, 60x oil/1.35 NA), Zeiss LSM510 Confocal (lenses: 10x/0.3 NA, 20x/0.8 NA, 40x/0.75 NA, 40x oil/1.30 NA), or

Zeiss LSM800 Confocal (lenses: 10x/0.3 NA, 20x/0.8 NA, 40x oil/1.3 NA). ICs were scored as described in [76].

Testis squashes

Internal reproductive organs were dissected from newly eclosed males in PBS, placed in a drop of PBS on a coverslip and punctured. A glass microscope slide was placed on top of the coverslip to squash the testes, and phase-contrast images were collected within 30 min of dissection using an Olympus IX-71 inverted microscope with Nikon Digital Sight camera with DS-U2 controller (20x lens/0.40 NA).

Fertility tests

For male fertility tests, ten males of each genotype were mated individually to two 3–4 day old *yw* virgin females at 23˚C. The males were discarded after one day, and the females were transferred to fresh vials each day for three more days and discarded on day 5. Progeny per vial were counted and averaged.

For homozygous female fertility tests, ten virgin females of each genotype were mated individually to two *yw* males at 23˚C. All flies were 3 days old at the time of mating. For hemizygous female fertility tests, virgin females less than one week old were mated to 1-day old w^{1118} males at 23˚C. The males were discarded after one day, and the females were transferred to fresh vials each day for three more days and discarded on day 5. Progeny per vial were counted and averaged.

For egg laying tests, 20 virgin mutant or control females were mated individually to one 7-day old w^{1118} male each at 23˚C. Young females were 7 days old at the time of mating; aged females were 18–19 days old at the time of mating. The males were discarded after one day, and the females were transferred to fresh vials each day for three more days and discarded on day 5. Eggs per vial were counted daily.

Maternal lethality tests were conducted by mating 20–25 young (<10 day old) $iPLA_2$-$VIA^{\Delta 23}$ or isogenic control females to control males and transferring them to cages with grape juice plates and live yeast paste overnight at 23˚C. After 20 hours of egg-laying, 90–120 eggs from each genotype were collected per experiment and moved to new plates at 23˚C. Larvae were collected and counted every 24 hours at 23˚C. Third instar larvae were moved to vials, and pupae were counted at 23˚C. The results of three experiments were averaged.

Mito-YFP quantification

$iPLA_2$-$VIA^{\Delta 23}$ mutant (*Psqh-mito-EYFP*, $iPLA_2$-$VIA^{\Delta 23}$/$iPLA_2$-$VIA^{\Delta 23}$), heterozygote (*Psqh-mito-EYFP*, $iPLA_2$-$VIA^{\Delta 23}$/*revertantΔ11*), and control females (*Psqh-mito-EYFP/revertantΔ11*) expressing *Psqh-mito-EYFP* were aged in groups of 10–20 flies at 23˚C. Females were mated to males on live yeast paste 1–2 days before dissection. Ovaries were dissected and stained with anti-GFP antibodies as described above. Every stage 8 or 9 egg chamber from each sample was photographed using identical confocal settings and 40x oil objective. After drawing an ROI around the nurse cell area and removing background signal with the same threshold, each image was converted to binary in ImageJ. Each binary image was converted to outlines, and the raw integrated density was measured for the ROI.

JC-1 fluorimetry

18–30 ovaries per sample were dissected from age-matched $iPLA_2$-$VIA^{\Delta 23}$ mutant, heterozygote, and control flies (genotypes and aging conditions as above). Tissues were immediately

transferred to cold 1x PBS. Sigma mitochondrial isolation kit (Sigma, MITOISO1) was used to extract mitochondria and perform the JC-1 assay according to the manufacturer's protocol, as follows. After discarding the PBS, each tissue sample was rinsed twice with cooled 1x Extraction Buffer using a glass Pasteur pipet. In a 3 ml glass homogenizer, the lysate was prepared in 1 mL of cooled 1x Extraction Buffer containing 2 mg/ml albumin and transferred to a microcentrifuge tube. The lysate was spun at 1000 x g for 5 minutes at 4˚C to remove cell debris, and the transferred supernatant was spun at 13,000 x g for 10 minutes at 4˚C to obtain the mitochondrial pellet. The pellet was resuspended in cooled 1x Extraction Buffer (without albumin) by pipetting, and the two centrifugation steps were repeated to get the mitochondria-enriched pellet, which was resuspended in cooled 1x Storage Buffer and stored on ice for immediate use or at 4˚C for a maximum of 24 hours. Mitochondrial protein concentration was determined by Bradford assay using a Beckman DU800 spectrophotometer. Sample concentrations were equilibrated with storage buffer. JC-1 assays were performed in clear bottom 96-well plates using a Beckman Coulter DTX800 spectrofluorometer. Each JC-1 reaction mixture of 100 μl was prepared with the same amount of mitochondrial sample (5–7 μg of mitochondrial protein per reaction), 1 μl of the JC-1 solution (final concentration 10 μg/ml) and 0.5 μl of the electron transport chain complex III inhibitor Antimycin A (final concentration 200 μg/ml) or 0.5 μl of the vehicle DMSO. Three technical replicates were prepared for each sample along with a blank lacking mitochondrial sample. After 10 minutes in the dark at room temperature, fluorescence intensity was measured using excitation wavelength of 485 nm, emission wavelength of 595 nm, and integration time of 1000 ms. The average fluorescence per mg of protein of each biological sample was calculated across technical replicates and converted to relative percentage of the isogenic control. For each genotype, 3–4 biological replicates were averaged.

Western blot

An equal number of adult flies for each sample were collected and frozen in liquid N_2. Frozen flies were homogenized in lysis buffer with Tris pH 7.5, NaCl, EDTA, NP40, DTT, NaF, and protease inhibitor cocktail (Roche), centrifuged to remove carcasses, and mixed with Laemmli buffer. Protein preps were run on a 10% SDS-PAGE gel, transferred to nitrocellulose (Bio-Rad), and blotted with mouse anti-HA (1:1000, Covance, MMS-101P) and mouse anti-beta-tubulin (1:2000, BioLegend, 903401). Secondary antibody was IRDye 800CW donkey anti-mouse IgG (Li-Cor, 925–32212). Quantifications were performed using Li-Cor Odyssey software.

Supporting information

S1 Fig. *iPLA$_2$-VIA* mRNA levels are unchanged by genetic perturbation of phospholipid metabolism genes. (A) Whole fly reverse transcription (RT) PCR shows no upregulation of *iPLA$_2$-VIA* mRNA expression when Pcyt1 is overexpressed using *tubulin-GAL4*. Control siblings lack the *tubulin-GAL4* driver. *pcyt1* mRNA upregulation is shown in the bottom panel of the gel image. (B-C) Whole fly RT-PCR shows no downregulation of *iPLA$_2$-VIA* expression in either the $pcyt1^{16919}$ mutant compared to w^{1118} (B) or in the eas^{KO} mutant compared to isogenic controls (C). Experiments were performed in triplicate. Quantifications were taken with Bio-Rad ImageLab 5.0, shown below representative gel images. Graphs show the ratio of *iPLA$_2$-VIA* mRNA normalized to internal control *actin* mRNA in each mutant genotype compared to the control genotype, averaged across three biological replicates. Error bars are standard deviations. (E-G) Whole fly RT-qPCR confirms that *iPLA$_2$-VIA* mRNA levels are not significantly different from controls when (E) Pcyt1 is overexpressed using *tubulin-GAL4*, (F) in $pcyt1^{16919}$ mutants, or (G) in eas^{KO} mutants. *iPLA$_2$-VIA* mRNA abundance was normalized

to *rp49* mRNA abundance ($2^{-\Delta Ct}$) and averaged across three biological replicates. Error bars are standard deviations. Statistical analysis by unpaired t-test (A, C, E-G) or single factor ANOVA (B), n.s. not significant.
(TIF)

S2 Fig. Transgenic catalytic-dead iPLA$_2$-VIA is expressed at lower levels than transgenic wild-type iPLA$_2$-VIA. Five male and five female adult flies were collected for each of the following genotypes: *tubulin-GAL4 > UAS-iPLA$_2$-VIA-PB-WT; tubulin-GAL4 > UAS-iPLA$_2$-VIA-PB-SA; tubulin-GAL4* alone. All three samples were processed in parallel, run on a denaturing SDS-PAGE gel, and blotted with both anti-HA to detect transgenic iPLA$_2$-VIA-HA and with anti-beta-tubulin as a loading control. Representative blot shown in (A), quantification of three biological replicates shown in (B). iPLA$_2$-VIA protein levels were normalized to beta-tubulin levels in each lane. Biological replicates are indicated by the gray circles, the average normalized protein levels are represented by the black bars, and error bars are standard deviations.
(TIF)

S3 Fig. Control RNA in situ hybridizations. (A) Riboprobe antisense to *wg* transcript (arrows) was used to demonstrate the fidelity of imaginal disc in situ hybridizations. (B) Riboprobe antisense to *cycB* transcript was used to demonstrate fidelity of testis in situ hybridizations. Arrows indicate staining in primary spermatocytes, and arrowheads indicate meiotic spermatids. (C) The *cycB* riboprobe also revealed specific expression in the larval brain (arrows). Scale bars: 100 μm.
(TIF)

S4 Fig. No maternal effect lethality in *iPLA$_2$-VIA$^{\Delta 23}$* mutants. Young (<10 day old) homozygous *iPLA$_2$-VIA$^{\Delta 23}$* females or isogenic control females were mated to control males and allowed to lay eggs on grape juice plates for 20 hours at 23˚C. First instar larvae hatched from isolated eggs were counted (black bars). Second instar larvae molted from isolated first instars were counted (dark gray bars). Third instar larvae molted from isolated second instars were counted (medium gray bars). Pupae were counted from isolated third instars (light gray bars). The entire experiment was repeated three times. Bars represent the average percentage of individuals that progress to each stage in the three experiments. Error bars are standard deviations. No developmental lethality is observed in progeny from *iPLA$_2$-VIA$^{\Delta 23}$* mutant mothers compared to control mothers.
(TIF)

S5 Fig. Mitochondrial aggregation is characteristic of aged *iPLA$_2$-VIA$^{\Delta 23}$* mutant germ cells. (A-B) Neither the parental stock carrying homozygous *Psqh-mito-EYFP* (A) nor *iPLA$_2$-VIA$^{\Delta 23}$* heterozygotes (B, *Psqh-mito-EYFP*, *iPLA$_2$-VIA$^{\Delta 23}$/revertantΔ11*) show mitochondrial clumping even at 6 weeks of age (white, mito-YFP; magenta, DAPI). (C-D) Mitochondrial clumping also is observed with another marker, immunofluorescence to ATP-5A protein in *iPLA$_2$-VIA$^{\Delta 23}$* mutants (D) but not in isogenic controls (C) at five weeks of age (white, anti-ATP-5A; magenta, DAPI). Magnified views of the boxed regions are shown in the insets. (E-F) Additionally, the ATP-5A signal is weaker in *iPLA$_2$-VIA$^{\Delta 23}$* mutants (dark red bars) than in age-matched controls (dark gray bars) at four (E) and five (F) weeks of age, possibly indicating mitochondrial degradation in the mutant. Bars represent averages, error bars are standard deviations. Statistical comparison by unpaired t-test. Scale bars: 20 μm.
(TIF)

S6 Fig. iPLA$_2$-VIA-PB localizes to Golgi in somatic larval tissues. HA-tagged wild-type iPLA$_2$-VIA-PB transgenic protein appears in puncta (green, A"-F", expressed with *tubulin-*

GAL4) that colocalize with a Golgi marker (red, anti-Golgin 84) in larval fat body (A) and salivary glands (D). Colocalization with an ER marker (red, B, E, anti-Calnexin 99A) and a mitochondrial marker (red, C, F, *UAS-mCherry-mitoOMM*) is weak or undetectable in these larval tissues. Scale bars: 20 μm.
(TIF)

S1 File. Raw gel and blot images.
(PDF)

Acknowledgments

We are grateful to the Bloomington *Drosophila* Stock Center, Kyoto *Drosophila* Genomics and Genetic Resource Center, Developmental Studies Hybridoma Bank, *Drosophila* Genomics Resource Center, Jessica Treisman, Yukiko Yamashita, Ruth Lehmann, the Jan lab, Michael Schlame, and Mindong Ren for fly stocks. We are grateful, as always, to Flybase, for its continual support of the *Drosophila* community. Sarah Liberow, Nicole Soussana, and Eliezer Heller assisted with some of the experiments. Critical comments on the manuscript were provided by Jessica Treisman and Rebecca Delventhal.

Author Contributions

Conceptualization: Josefa Steinhauer.

Formal analysis: Surya Jyoti Banerjee, Josefa Steinhauer.

Funding acquisition: Josefa Steinhauer.

Investigation: Surya Jyoti Banerjee, Adina Schonbrun, Sogol Eizadshenass, Shimshon Benji, Yaakov Tzvi Cantor, Liam Eliach, Matthew Lubin, Zev Narrowe, Jeremy Purow, Benjamin Shulman, Leib Wiener, Josefa Steinhauer.

Methodology: Surya Jyoti Banerjee, Adina Schonbrun, Josefa Steinhauer.

Project administration: Josefa Steinhauer.

Resources: Josefa Steinhauer.

Supervision: Surya Jyoti Banerjee, Josefa Steinhauer.

Visualization: Josefa Steinhauer.

Writing – original draft: Josefa Steinhauer.

Writing – review & editing: Surya Jyoti Banerjee, Adina Schonbrun, Josefa Steinhauer.

References

1. Wyss-Coray T. Ageing, neurodegeneration and brain rejuvenation. Nature. 2016; 539(7628):180–6. https://doi.org/10.1038/nature20411 PMID: 27830812; PubMed Central PMCID: PMC5172605.
2. Katsnelson A, De Strooper B, Zoghbi HY. Neurodegeneration: From cellular concepts to clinical applications. Sci Transl Med. 2016; 8(364):364ps18. https://doi.org/10.1126/scitranslmed.aal2074 PMID: 27831899.
3. Erkkinen MG, Kim MO, Geschwind MD. Clinical Neurology and Epidemiology of the Major Neurodegenerative Diseases. Cold Spring Harb Perspect Biol. 2018; 10(4). https://doi.org/10.1101/cshperspect.a033118 PMID: 28716886; PubMed Central PMCID: PMC5880171.
4. Langston JW, Ballard P, Tetrud JW, Irwin I. Chronic Parkinsonism in humans due to a product of meperidine-analog synthesis. Science. 1983; 219(4587):979–80. https://doi.org/10.1126/science.6823561 PMID: 6823561.

5. Betarbet R, Sherer TB, MacKenzie G, Garcia-Osuna M, Panov AV, Greenamyre JT. Chronic systemic pesticide exposure reproduces features of Parkinson's disease. Nat Neurosci. 2000; 3(12):1301–6. https://doi.org/10.1038/81834 PMID: 11100151.

6. Brooks AI, Chadwick CA, Gelbard HA, Cory-Slechta DA, Federoff HJ. Paraquat elicited neurobehavioral syndrome caused by dopaminergic neuron loss. Brain Res. 1999; 823(1–2):1–10. https://doi.org/10.1016/s0006-8993(98)01192-5 PMID: 10095006.

7. Henchcliffe C, Beal MF. Mitochondrial biology and oxidative stress in Parkinson disease pathogenesis. Nat Clin Pract Neurol. 2008; 4(11):600–9. https://doi.org/10.1038/ncpneuro0924 PMID: 18978800.

8. Kamel F. Epidemiology. Paths from pesticides to Parkinson's. Science. 2013; 341(6147):722–3. https://doi.org/10.1126/science.1243619 PMID: 23950519.

9. Trinh J, Farrer M. Advances in the genetics of Parkinson disease. Nat Rev Neurol. 2013; 9(8):445–54. Epub 2013/07/16. https://doi.org/10.1038/nrneurol.2013.132 PMID: 23857047.

10. Hewitt VL, Whitworth AJ. Mechanisms of Parkinson's Disease: Lessons from Drosophila. Curr Top Dev Biol. 2017; 121:173–200. https://doi.org/10.1016/bs.ctdb.2016.07.005 Epub 2016 Jul 30. PMID: 28057299.

11. Morgan NV, Westaway SK, Morton JE, Gregory A, Gissen P, Sonek S, et al. PLA2G6, encoding a phospholipase A2, is mutated in neurodegenerative disorders with high brain iron. Nat Genet. 2006; 38(7):752–4. https://doi.org/10.1038/ng1826 Epub 2006 Jun 18. PMID: 16783378; PubMed Central PMCID: PMC2117328.

12. Khateeb S, Flusser H, Ofir R, Shelef I, Narkis G, Vardi G, et al. PLA2G6 mutation underlies infantile neuroaxonal dystrophy. Am J Hum Genet. 2006; 79(5):942–8. https://doi.org/10.1086/508572 Epub 2006 Sep 19. PMID: 17033970; PubMed Central PMCID: PMC1698558.

13. Paisan-Ruiz C, Bhatia KP, Li A, Hernandez D, Davis M, Wood NW, et al. Characterization of PLA2G6 as a locus for dystonia-parkinsonism. Ann Neurol. 2009; 65(1):19–23. https://doi.org/10.1002/ana.21415 PMID: 18570303.

14. Gregory A, Kurian MA, Maher ER, Hogarth P, Hayflick SJ. PLA2G6-Associated Neurodegeneration. In: Adam MP, Ardinger HH, Pagon RA, Wallace SE, Bean LJH, Mefford HC, et al., editors. GeneReviews ((R)). Seattle (WA)1993.

15. Murakami M, Taketomi Y, Miki Y, Sato H, Hirabayashi T, Yamamoto K. Recent progress in phospholipase A(2) research: from cells to animals to humans. Prog Lipid Res. 2011; 50(2):152–92. https://doi.org/10.1016/j.plipres.2010.12.001 PMID: 21185866.

16. Lands WE. Stories about acyl chains. Biochim Biophys Acta. 2000; 1483(1):1–14. https://doi.org/10.1016/s1388-1981(99)00177-8 PMID: 10601692.

17. Ye C, Shen Z, Greenberg ML. Cardiolipin remodeling: a regulatory hub for modulating cardiolipin metabolism and function. J Bioenerg Biomembr. 2016; 48(2):113–23. https://doi.org/10.1007/s10863-014-9591-7 PMID: 25432572; PubMed Central PMCID: PMC4449329.

18. Bradley RM, Stark KD, Duncan RE. Influence of tissue, diet, and enzymatic remodeling on cardiolipin fatty acyl profile. Mol Nutr Food Res. 2016; 60(8):1804–18. https://doi.org/10.1002/mnfr.201500966 Epub 2016 May 17. PMID: 27061349.

19. Seleznev K, Zhao C, Zhang XH, Song K, Ma ZA. Calcium-independent phospholipase A2 localizes in and protects mitochondria during apoptotic induction by staurosporine. J Biol Chem. 2006; 281(31):22275–88. https://doi.org/10.1074/jbc.M604330200 PMID: 16728389; PubMed Central PMCID: PMC1829309.

20. Bao S, Li Y, Lei X, Wohltmann M, Jin W, Bohrer A, et al. Attenuated free cholesterol loading-induced apoptosis but preserved phospholipid composition of peritoneal macrophages from mice that do not express group VIA phospholipase A2. J Biol Chem. 2007; 282(37):27100–14. https://doi.org/10.1074/jbc.M701316200 PMID: 17627946; PubMed Central PMCID: PMC2044506.

21. Song H, Bao S, Lei X, Jin C, Zhang S, Turk J, et al. Evidence for proteolytic processing and stimulated organelle redistribution of iPLA(2)beta. Biochim Biophys Acta. 2010; 1801(5):547–58. https://doi.org/10.1016/j.bbalip.2010.01.006 PMID: 20132906; PubMed Central PMCID: PMC2848069.

22. Song H, Wohltmann M, Tan M, Ladenson JH, Turk J. Group VIA phospholipase A2 mitigates palmitate-induced beta-cell mitochondrial injury and apoptosis. J Biol Chem. 2014; 289(20):14194–210. https://doi.org/10.1074/jbc.M114.561910 Epub 2014 Mar 19. PMID: 24648512; PubMed Central PMCID: PMC4022886.

23. Malhotra A, Edelman-Novemsky I, Xu Y, Plesken H, Ma J, Schlame M, et al. Role of calcium-independent phospholipase A2 in the pathogenesis of Barth syndrome. Proc Natl Acad Sci U S A. 2009; 106(7):2337–41. https://doi.org/10.1073/pnas.0811224106 Epub 2009 Jan 21. PMID: 19164547; PubMed Central PMCID: PMC2650157.

24. Hsu YH, Dumlao DS, Cao J, Dennis EA. Assessing phospholipase A2 activity toward cardiolipin by mass spectrometry. PLoS One. 2013; 8(3):e59267. https://doi.org/10.1371/journal.pone.0059267 Epub 2013 Mar 22. PMID: 23533611; PubMed Central PMCID: PMC3606342.

25. Zhao Z, Zhang X, Zhao C, Choi J, Shi J, Song K, et al. Protection of pancreatic beta-cells by group VIA phospholipase A(2)-mediated repair of mitochondrial membrane peroxidation. Endocrinology. 2010; 151(7):3038–48. https://doi.org/10.1210/en.2010-0016 PMID: 20463052; PubMed Central PMCID: PMC2903934.

26. Kinghorn KJ, Castillo-Quan JI, Bartolome F, Angelova PR, Li L, Pope S, et al. Loss of PLA2G6 leads to elevated mitochondrial lipid peroxidation and mitochondrial dysfunction. Brain. 2015; 138(Pt 7):1801–16. https://doi.org/10.1093/brain/awv132 Epub 2015 May 22. PMID: 26001724; PubMed Central PMCID: PMC4559908.

27. Beck G, Sugiura Y, Shinzawa K, Kato S, Setou M, Tsujimoto Y, et al. Neuroaxonal dystrophy in calcium-independent phospholipase A2beta deficiency results from insufficient remodeling and degeneration of mitochondrial and presynaptic membranes. J Neurosci. 2011; 31(31):11411–20. https://doi.org/10.1523/JNEUROSCI.0345-11.2011 PMID: 21813701.

28. Chiu CC, Lu CS, Weng YH, Chen YL, Huang YZ, Chen RS, et al. PARK14 (D331Y) PLA2G6 Causes Early-Onset Degeneration of Substantia Nigra Dopaminergic Neurons by Inducing Mitochondrial Dysfunction, ER Stress, Mitophagy Impairment and Transcriptional Dysregulation in a Knockin Mouse Model. Mol Neurobiol. 2019; 56(6):3835–53. https://doi.org/10.1007/s12035-018-1118-5 Epub 2018 Aug 8. PMID: 30088174.

29. Chiu CC, Yeh TH, Lu CS, Huang YC, Cheng YC, Huang YZ, et al. PARK14 PLA2G6 mutants are defective in preventing rotenone-induced mitochondrial dysfunction, ROS generation and activation of mitochondrial apoptotic pathway. Oncotarget. 2017; 8(45):79046–60. https://doi.org/10.18632/oncotarget.20893 eCollection 2017 Oct 3. PMID: 29108286; PubMed Central PMCID: PMC5668019.

30. Schlame M, Blais S, Edelman-Novemsky I, Xu Y, Montecillo F, Phoon CK, et al. Comparison of cardiolipins from Drosophila strains with mutations in putative remodeling enzymes. Chem Phys Lipids. 2012; 165(5):512–9. https://doi.org/10.1016/j.chemphyslip.2012.03.001 Epub 2012 Mar 23. PMID: 22465155.

31. Turk J, White TD, Nelson AJ, Lei X, Ramanadham S. iPLA2beta and its role in male fertility, neurological disorders, metabolic disorders, and inflammation. Biochim Biophys Acta Mol Cell Biol Lipids. 2019; 1864(6):846–60. https://doi.org/10.1016/j.bbalip.2018.10.010 Epub 2018 Nov 5. PMID: 30408523; PubMed Central PMCID: PMC6432790.

32. Malley KR, Koroleva O, Miller I, Sanishvili R, Jenkins CM, Gross RW, et al. The structure of iPLA2beta reveals dimeric active sites and suggests mechanisms of regulation and localization. Nat Commun. 2018; 9(1):765. https://doi.org/10.1038/s41467-018-03193-0 PMID: 29472584; PubMed Central PMCID: PMC5823874.

33. Balsinde J, Balboa MA. Cellular regulation and proposed biological functions of group VIA calcium-independent phospholipase A2 in activated cells. Cell Signal. 2005; 17(9):1052–62. https://doi.org/10.1016/j.cellsig.2005.03.002 PMID: 15993747.

34. Zhou Q, Yen A, Rymarczyk G, Asai H, Trengrove C, Aziz N, et al. Impairment of PARK14-dependent Ca(2+) signalling is a novel determinant of Parkinson's disease. Nat Commun. 2016; 7:10332. https://doi.org/10.1038/ncomms10332 PMID: 26755131; PubMed Central PMCID: PMC4729940.

35. Bao S, Jin C, Zhang S, Turk J, Ma Z, Ramanadham S. Beta-cell calcium-independent group VIA phospholipase A(2) (iPLA(2)beta): tracking iPLA(2)beta movements in response to stimulation with insulin secretagogues in INS-1 cells. Diabetes. 2004; 53 Suppl 1:S186–9. https://doi.org/10.2337/diabetes.53.2007.s186 PMID: 14749286; PubMed Central PMCID: PMC3761941.

36. Iliadi KG, Gluscencova OB, Iliadi N, Boulianne GL. Mutations in the Drosophila homolog of human PLA2G6 give rise to age-dependent loss of psychomotor activity and neurodegeneration. Sci Rep. 2018; 8(1):2939. https://doi.org/10.1038/s41598-018-21343-8 PMID: 29440694; PubMed Central PMCID: PMC5811537.

37. Mori A, Hatano T, Inoshita T, Shiba-Fukushima K, Koinuma T, Meng H, et al. Parkinson's disease-associated iPLA2-VIA/PLA2G6 regulates neuronal functions and alpha-synuclein stability through membrane remodeling. Proc Natl Acad Sci U S A. 2019; 116(41):20689–99. Epub 2019/09/23. https://doi.org/10.1073/pnas.1902958116 PMID: 31548400; PubMed Central PMCID: PMC6789907.

38. Bao S, Miller DJ, Ma Z, Wohltmann M, Eng G, Ramanadham S, et al. Male mice that do not express group VIA phospholipase A2 produce spermatozoa with impaired motility and have greatly reduced fertility. J Biol Chem. 2004; 279(37):38194–200. https://doi.org/10.1074/jbc.M406489200 PMID: 15252026; PubMed Central PMCID: PMC3733543.

39. Lin G, Lee PT, Chen K, Mao D, Tan KL, Zuo Z, et al. Phospholipase PLA2G6, a Parkinsonism-Associated Gene, Affects Vps26 and Vps35, Retromer Function, and Ceramide Levels, Similar to alpha-Synuclein Gain. Cell Metab. 2018; 28(4):605–18 e6. https://doi.org/10.1016/j.cmet.2018.05.019 PMID: 29909971.

40. Baburina I, Jackowski S. Cellular responses to excess phospholipid. J Biol Chem. 1999; 274(14):9400–8. https://doi.org/10.1074/jbc.274.14.9400 PMID: 10092620.

41. Barbour SE, Kapur A, Deal CL. Regulation of phosphatidylcholine homeostasis by calcium-independent phospholipase A2. Biochim Biophys Acta. 1999; 1439(1):77–88. https://doi.org/10.1016/s1388-1981(99)00078-5 PMID: 10395967.

42. Weber U, Eroglu C, Mlodzik M. Phospholipid membrane composition affects EGF receptor and Notch signaling through effects on endocytosis during Drosophila development. Dev Cell. 2003; 5(4):559–70. https://doi.org/10.1016/s1534-5807(03)00273-9 PMID: 14536058.

43. Fernández-Murray JP, McMaster CR. Phosphatidylcholine synthesis and its catabolism by yeast neuropathy target esterase 1. Biochim Biophys Acta. 2007; 1771(3):331–6. Epub 2006/05/12. https://doi.org/10.1016/j.bbalip.2006.04.004 PMID: 16731034.

44. Meltzer S, Bagley JA, Perez GL, O'Brien CE, DeVault L, Guo Y, et al. Phospholipid Homeostasis Regulates Dendrite Morphogenesis in Drosophila Sensory Neurons. Cell Rep. 2017; 21(4):859–66. https://doi.org/10.1016/j.celrep.2017.09.089 PMID: 29069593; PubMed Central PMCID: PMC5687885.

45. Ali YO, Escala W, Ruan K, Zhai RG. Assaying locomotor, learning, and memory deficits in Drosophila models of neurodegeneration. J Vis Exp. 2011;(49). https://doi.org/10.3791/2504 PMID: 21445036; PubMed Central PMCID: PMC3197301.

46. Kienesberger PC, Oberer M, Lass A, Zechner R. Mammalian patatin domain containing proteins: a family with diverse lipolytic activities involved in multiple biological functions. J Lipid Res. 2009; 50 Suppl: S63–8. Epub 2008/11/23. https://doi.org/10.1194/jlr.R800082-JLR200 PMID: 19029121; PubMed Central PMCID: PMC2674697.

47. Engel LA, Jing Z, O'Brien DE, Sun M, Kotzbauer PT. Catalytic function of PLA2G6 is impaired by mutations associated with infantile neuroaxonal dystrophy but not dystonia-parkinsonism. PLoS One. 2010; 5(9):e12897. https://doi.org/10.1371/journal.pone.0012897 PMID: 20886109; PubMed Central PMCID: PMC2944820.

48. Clark IE, Dodson MW, Jiang C, Cao JH, Huh JR, Seol JH, et al. Drosophila pink1 is required for mitochondrial function and interacts genetically with parkin. Nature. 2006; 441(7097):1162–6. Epub 2006/05/03. https://doi.org/10.1038/nature04779 PMID: 16672981.

49. Park J, Lee SB, Lee S, Kim Y, Song S, Kim S, et al. Mitochondrial dysfunction in Drosophila PINK1 mutants is complemented by parkin. Nature. 2006; 441(7097):1157–61. Epub 2006/05/03. https://doi.org/10.1038/nature04788 PMID: 16672980.

50. Maruzs T, Simon-Vecsei Z, Kiss V, Csizmadia T, Juhász G. On the Fly: Recent Progress on Autophagy and Aging in Drosophila. Front Cell Dev Biol. 2019; 7:140. Epub 2019/07/24. https://doi.org/10.3389/fcell.2019.00140 PMID: 31396511; PubMed Central PMCID: PMC6667644.

51. Schlame M. Cardiolipin remodeling and the function of tafazzin. Biochim Biophys Acta. 2013; 1831(3):582–8. https://doi.org/10.1016/j.bbalip.2012.11.007 PMID: 23200781.

52. Fabrizio JJ, Hime G, Lemmon SK, Bazinet C. Genetic dissection of sperm individualization in Drosophila melanogaster. Development. 1998; 125(10):1833–43. PMID: 9550716.

53. Narendra D, Kane LA, Hauser DN, Fearnley IM, Youle RJ. p62/SQSTM1 is required for Parkin-induced mitochondrial clustering but not mitophagy; VDAC1 is dispensable for both. Autophagy. 2010; 6(8):1090–106. https://doi.org/10.4161/auto.6.8.13426 PMID: 20890124; PubMed Central PMCID: PMC3359490.

54. Okatsu K, Saisho K, Shimanuki M, Nakada K, Shitara H, Sou YS, et al. p62/SQSTM1 cooperates with Parkin for perinuclear clustering of depolarized mitochondria. Genes Cells. 2010; 15(8):887–900. Epub 2010/07/02. https://doi.org/10.1111/j.1365-2443.2010.01426.x PMID: 20604804; PubMed Central PMCID: PMC2970908.

55. Riedel F, Gillingham AK, Rosa-Ferreira C, Galindo A, Munro S. An antibody toolkit for the study of membrane traffic in Drosophila melanogaster. Biol Open. 2016; 5(7):987–92. https://doi.org/10.1242/bio.018937 PMID: 27256406; PubMed Central PMCID: PMC4958275.

56. Manguikian AD, Barbour SE. Cell cycle dependence of group VIA calcium-independent phospholipase A2 activity. J Biol Chem. 2004; 279(51):52881–92. https://doi.org/10.1074/jbc.M410659200 PMID: 15385540.

57. Pavlidis P, Ramaswami M, Tanouye MA. The Drosophila easily shocked gene: a mutation in a phospholipid synthetic pathway causes seizure, neuronal failure, and paralysis. Cell. 1994; 79(1):23–33. https://doi.org/10.1016/0092-8674(94)90397-2 PMID: 7923374.

58. Baker NE. Patterning signals and proliferation in Drosophila imaginal discs. Curr Opin Genet Dev. 2007; 17(4):287–93. https://doi.org/10.1016/j.gde.2007.05.005 PMID: 17624759.

59. Schlame M, Xu Y, Ren M. The Basis for Acyl Specificity in the Tafazzin Reaction. J Biol Chem. 2017; 292(13):5499–506. https://doi.org/10.1074/jbc.M116.769182 PMID: 28202545; PubMed Central PMCID: PMC5392692.

60. Cox RT, Spradling AC. Clueless, a conserved Drosophila gene required for mitochondrial subcellular localization, interacts genetically with parkin. Dis Model Mech. 2009; 2(9–10):490–9. Epub 2009/07/28. https://doi.org/10.1242/dmm.002378 PMID: 19638420; PubMed Central PMCID: PMC2737057.

61. Sen A, Kalvakuri S, Bodmer R, Cox RT. Clueless, a protein required for mitochondrial function, interacts with the PINK1-Parkin complex in Drosophila. Dis Model Mech. 2015; 8(6):577–89. Epub 2015/04/20. https://doi.org/10.1242/dmm.019208 PMID: 26035866; PubMed Central PMCID: PMC4457034.

62. Lieber T, Jeedigunta SP, Palozzi JM, Lehmann R, Hurd TR. Mitochondrial fragmentation drives selective removal of deleterious mtDNA in the germline. Nature. 2019; 570(7761):380–4. Epub 2019/05/15. https://doi.org/10.1038/s41586-019-1213-4 PMID: 31092924; PubMed Central PMCID: PMC6614061.

63. Villa E, Marchetti S, Ricci JE. No Parkin Zone: Mitophagy without Parkin. Trends Cell Biol. 2018; 28 (11):882–95. Epub 2018/08/13. https://doi.org/10.1016/j.tcb.2018.07.004 PMID: 30115557.

64. Shinzawa K, Sumi H, Ikawa M, Matsuoka Y, Okabe M, Sakoda S, et al. Neuroaxonal dystrophy caused by group VIA phospholipase A2 deficiency in mice: a model of human neurodegenerative disease. J Neurosci. 2008; 28(9):2212–20. https://doi.org/10.1523/JNEUROSCI.4354-07.2008 PMID: 18305254.

65. Mori A, Hatano T, Inoshita T, Shiba-Fukushima K, Koinuma T, Meng H, et al. Parkinson's disease-associated. Proc Natl Acad Sci U S A. 2019; 116(41):20689–99. Epub 2019/09/23. https://doi.org/10.1073/pnas.1902958116 PMID: 31548400; PubMed Central PMCID: PMC6789907.

66. Wada H, Yasuda T, Miura I, Watabe K, Sawa C, Kamijuku H, et al. Establishment of an improved mouse model for infantile neuroaxonal dystrophy that shows early disease onset and bears a point mutation in Pla2g6. Am J Pathol. 2009; 175(6):2257–63. https://doi.org/10.2353/ajpath.2009.090343 Epub 2009 Nov 5. PMID: 19893029; PubMed Central PMCID: PMC2789634.

67. Malik I, Turk J, Mancuso DJ, Montier L, Wohltmann M, Wozniak DF, et al. Disrupted membrane homeostasis and accumulation of ubiquitinated proteins in a mouse model of infantile neuroaxonal dystrophy caused by PLA2G6 mutations. Am J Pathol. 2008; 172(2):406–16. https://doi.org/10.2353/ajpath.2008.070823 Epub 2008 Jan 17. PMID: 18202189; PubMed Central PMCID: PMC2312364.

68. Salih MA, Mundwiller E, Khan AO, AlDrees A, Elmalik SA, Hassan HH, et al. New findings in a global approach to dissect the whole phenotype of PLA2G6 gene mutations. PLoS One. 2013; 8(10):e76831. Epub 2013/10/09. https://doi.org/10.1371/journal.pone.0076831 PMID: 24130795; PubMed Central PMCID: PMC3792983.

69. Pickles S, Vigié P, Youle RJ. Mitophagy and Quality Control Mechanisms in Mitochondrial Maintenance. Curr Biol. 2018; 28(4):R170–R85. https://doi.org/10.1016/j.cub.2018.01.004 PMID: 29462587; PubMed Central PMCID: PMC7255410.

70. Riparbelli MG, Callaini G. The Drosophila parkin homologue is required for normal mitochondrial dynamics during spermiogenesis. Dev Biol. 2007; 303(1):108–20. Epub 2006/11/10. https://doi.org/10.1016/j.ydbio.2006.10.038 PMID: 17123504.

71. Xu Y, Condell M, Plesken H, Edelman-Novemsky I, Ma J, Ren M, et al. A Drosophila model of Barth syndrome. Proc Natl Acad Sci U S A. 2006; 103(31):11584–8. https://doi.org/10.1073/pnas.0603242103 PMID: 16855048; PubMed Central PMCID: PMC1544213.

72. Delventhal R, Steinhauer J. A course-based undergraduate research experience examining neurodegeneration in Drosophila melanogaster teaches students to think, communicate, and perform like scientists. PLoS One. 2020; 15(4):e0230912. Epub 2020/04/13. https://doi.org/10.1371/journal.pone.0230912 PMID: 32282825; PubMed Central PMCID: PMC7153876.

73. Nagaso H, Murata T, Day N, Yokoyama KK. Simultaneous detection of RNA and protein by in situ hybridization and immunological staining. J Histochem Cytochem. 2001; 49(9):1177–82. https://doi.org/10.1177/002215540104900911 PMID: 11511686.

74. Steinhauer J, Kalderon D. The RNA-binding protein Squid is required for the establishment of anteroposterior polarity in the Drosophila oocyte. Development. 2005; 132(24):5515–25. https://doi.org/10.1242/dev.02159 PMID: 16291786.

75. Morris CA, Benson E, White-Cooper H. Determination of gene expression patterns using in situ hybridization to Drosophila testes. Nat Protoc. 2009; 4(12):1807–19. https://doi.org/10.1038/nprot.2009.192 PMID: 20010932.

76. Ben-David G, Miller E, Steinhauer J. Drosophila spermatid individualization is sensitive to temperature and fatty acid metabolism. Spermatogenesis. 2015; 5(1):e1006089. https://doi.org/10.1080/21565562.2015.1006089 PMID: 26413411; PubMed Central PMCID: PMC4581069.